https://doi.org/10.5194/egusphere-2026-5006
Preprint. Discussion started: 31 August 2026

Background-state dependence of aerosol responses in CESM2 boreal-summer climate

Tianhui Zhou[1], Massimo A. Bollasina[1]

[1]School of GeoSciences, University of Edinburgh, Edinburgh, UK

Correspondence to: Tianhui Zhou (T.Zhou-16@sms.ed.ac.uk)

Abstract. Anthropogenic aerosol forcing is commonly estimated using aerosol-only single-forcing experiments, but can also be inferred as a residual from all-forcing and fixed-aerosol simulations. Although previous studies have demonstrated nonlinear interactions among climate forcings, it remains unclear whether these approaches provide dynamically equivalent aerosol responses, particularly at regional scale. Here, we compare the directly simulated aerosol response (AAER) with the residual estimate (ALL−xAER) in Community Earth System Model version 2 (CESM2) across two contrasting periods: 1965–1985 relative to 1920–1940, representing the historical increase in anthropogenic aerosol loading, and 2030–2050 relative to 1965–1985, representing the subsequent decline and geographical redistribution of aerosol emissions. We focus on boreal summer, when aerosol forcing strongly interacts with monsoon circulation and large-scale atmospheric dynamics.

During the historical transition, AAER and ALL−xAER produce broadly similar Northern Hemisphere responses, particularly in near-surface temperature, although regional differences occur in precipitation and circulation. During the future transition, the two estimates diverge substantially, especially in precipitation over the Indo-Pacific and Asian monsoon regions. These differences are associated with reorganised low-level moisture transport and upper-tropospheric circulation, including changes in jet structure, Rossby-wave propagation, and tropical–extratropical teleconnections. The North Atlantic exhibits an additional coupled ocean–atmosphere component, with different sea surface temperature and Atlantic Meridional Overturning Circulation responses between AAER and ALL−xAER. These results demonstrate that the two approaches are not dynamically interchangeable in CESM2: the diagnosed aerosol response depends on the evolving background climate state in which aerosol forcing operates, with important implications for residual-based attribution of regional climate change under future greenhouse-gas forcing.

1 Introduction

Human activities have substantially altered the atmospheric composition through emissions of greenhouse gases (GHGs) and anthropogenic aerosols (Meinshausen et al., 2017; Hoesly et al., 2018). These forcing agents influence the climate system through fundamentally different mechanisms. GHGs exert a relatively long-lived and spatially widespread warming influence, whereas anthropogenic aerosols are short-lived, spatially heterogeneous, and concentrated near major emission regions (Persad

https://doi.org/10.5194/egusphere-2026-5006
Preprint. Discussion started: 31 August 2026

and Caldeira, 2018; Samset et al., 2018). Through scattering and absorption of solar radiation and the modification of cloud microphysical properties, aerosols reduce surface insolation, alter atmospheric heating profiles, and affect precipitation and regional circulation. The IPCC Sixth Assessment Report identifies anthropogenic aerosols as one of the largest remaining uncertainties in anthropogenic radiative forcing. Although aerosol emissions have partially offset greenhouse-gas warming over the industrial period, their short atmospheric lifetimes and strong spatial heterogeneity produce pronounced regional contrasts in forcing and rapid responses to emission changes, contributing substantially to uncertainty in regional climate responses and their attribution (Bellouin et al., 2020; IPCC, 2021; Szopa et al., 2021).

Because of their heterogeneous forcing, aerosols can induce climate responses that differ substantially from those associated with well-mixed greenhouse gases. Increased anthropogenic aerosol loading generally cools the Northern Hemisphere relative to the Southern Hemisphere because major emission sources are concentrated in the Northern Hemisphere, perturbing meridional energy gradients and driving compensating changes in atmospheric and oceanic heat transport (Hwang et al., 2013; Allen et al., 2014; Needham and Randall, 2023; Needham et al., 2024). These adjustments modify large-scale circulation features, including the Hadley circulation, storm tracks, and the position of tropical rain belts (Hwang et al., 2013; Allen et al., 2014; Needham and Randall, 2023). Over the Asian monsoon region, aerosol-induced surface cooling weakens the land–sea thermal contrast, reducing the strength of the low-level monsoon circulation and moisture transport into the continent, thereby suppressing precipitation over South and East Asia (Bollasina et al., 2011; Li et al., 2016; Dong et al., 2019). Aerosol forcing can also excite stationary Rossby wave trains that propagate far from source regions, linking regional forcing to remote precipitation and circulation responses through atmospheric teleconnections (Shindell et al., 2012; Undorf et al., 2018; Shawki et al., 2018; Wilcox et al., 2019; Sun et al., 2026). Anthropogenic aerosols can therefore influence climate well beyond their emission regions through both hemispheric energy-balance adjustments and dynamical circulation pathways.

A central challenge in attributing climate responses to individual forcing agents is that the response in an all-forcing simulation reflects the combined influence of multiple anthropogenic and natural forcings and therefore does not directly identify the contribution of any individual driver. Two approaches are commonly used to isolate forcing-specific responses. The first relies on coordinated single-forcing experiments, in which simulations are driven separately by greenhouse gases, anthropogenic aerosols, or natural forcings, and has been widely applied in detection and attribution studies (Eyring et al., 2016; Gillett et al., 2016). The second estimates the contribution of a forcing using a residual approach, in which its effect is inferred from the difference between an all-forcing simulation and a corresponding experiment in which that forcing is held fixed or removed (e.g., Simpson et al., 2023). These approaches are often implicitly treated as equivalent estimates of the same forcing contribution. However, this equivalence is not guaranteed. A residual estimate diagnoses the response to a forcing in the presence of the other simultaneously evolving forcings and the associated background climate state, whereas a dedicated single-forcing experiment diagnoses the response to that forcing under a different background state. The two approaches will

https://doi.org/10.5194/egusphere-2026-5006
Preprint. Discussion started: 31 August 2026

therefore be equivalent only if the response to the forcing is sufficiently insensitive to the state in which it operates and to interactions with the other forcing agents.

This distinction is particularly important because forcing responses need not be linearly additive. Previous studies have shown that the combined response to greenhouse gases and anthropogenic aerosols can depart from the sum of their separately forced responses owing to interactions involving cloud processes, surface albedo, atmospheric structure, and ocean circulation (Feichter et al., 2004; Ming and Ramaswamy, 2009; Ming et al., 2011). More recent studies have demonstrated that such nonlinear residuals can be relatively small for some global-mean quantities, including surface temperature, precipitation, and top-of-atmosphere radiative fluxes, while remaining substantial at regional and seasonal scales (Deng et al., 2020). Apparent additivity at the global scale may therefore partly arise from cancellation between regional anomalies of opposite sign. Such nonlinear behaviour is particularly relevant to aerosol–GHG interactions because aerosols produce spatially heterogeneous forcing and interact with climate-state-dependent feedbacks involving sea ice, surface albedo, ocean circulation, and monsoon dynamics (Feichter et al., 2004; Ming and Ramaswamy, 2009; Deng et al., 2020; Simpson et al., 2023).

Early studies of forcing additivity similarly demonstrated that linear superposition provides a reasonable approximation for some large-scale temperature responses but performs less well for regional climate patterns (Mitchell et al., 1995; Gillett et al., 2004). Subsequent work has shown that greenhouse gases and aerosols can exert competing influences on regional hydroclimate by modifying land–sea thermal contrasts, monsoon circulation, and large-scale atmospheric dynamics, further complicating the separation of individual forcing contributions (Jones et al., 2016; Guo et al., 2013; Lau and Kim, 2017; Herbert et al., 2022; Recchia and Lucarini, 2023). These studies demonstrate that regional climate responses cannot always be interpreted as a simple linear combination of individual forcing effects. However, the question of forcing additivity is distinct from the question of whether different experimental approaches provide equivalent estimates of a particular forcing response. Even if the sum of separately forced responses approximately reproduces the all-forcing response, the aerosol contribution inferred as a residual need not reproduce the response obtained from a dedicated aerosol-only experiment.

This distinction provides the motivation for the present study. A residual-based aerosol estimate effectively represents the response to aerosol forcing conditional on the evolving influence of the other forcings and the background climate state. In contrast, an aerosol-only experiment isolates the response to aerosol forcing from a climate state that evolves in the absence of the other imposed forcings. Differences between the two estimates can therefore arise when the aerosol response depends on the state of the coupled climate system or when aerosol forcing interacts nonlinearly with other forcing agents. Such state dependence may be particularly important under future climate conditions, when greenhouse-gas-driven warming substantially alters the atmosphere–ocean system and can modify circulation, SST distributions, ocean feedbacks, and hydroclimate responses to aerosol forcing. Assessing the equivalence of direct and residual-based aerosol estimates is therefore essential for

https://doi.org/10.5194/egusphere-2026-5006
Preprint. Discussion started: 31 August 2026

interpreting forcing-specific attribution studies and for determining whether aerosol responses diagnosed using different experimental designs can be meaningfully compared.

Here, we use CESM2, which provides both a large all-forcing ensemble and coordinated single-forcing experiments within the same coupled model framework (Rodgers et al., 2021; Simpson et al., 2023). This experimental framework allows us to directly assess whether the response obtained from dedicated anthropogenic-aerosol-only simulations is dynamically equivalent to the aerosol contribution inferred from the difference between all-forcing and no-aerosol simulations. We focus on boreal summer (June–July–August, JJA), when land–sea thermal contrasts are strong, the Asian monsoon circulation is fully developed, and aerosol forcing can exert pronounced influences on circulation and hydroclimate. We examine two climate transitions representing different background states and aerosol-forcing regimes, and ask three related questions: (1) to what extent does the residual aerosol response reproduce the directly simulated aerosol response; (2) where and under which climate conditions do the two estimates diverge; and (3) what physical mechanisms account for these differences? By analysing the associated changes in surface climate, circulation, SSTs, and atmospheric teleconnections, we identify how the background climate state and forcing interactions shape the diagnosed aerosol response. Our results therefore provide a direct assessment of the extent to which residual and single-forcing approaches can be considered dynamically interchangeable, with implications for the interpretation of aerosol contributions to historical and future regional climate change.

2 Models, experiments, and methods

2.1 CESM2 and its single-forcing experiments

CESM2 is a fully coupled Earth system model developed by the National Center for Atmospheric Research (NCAR) and collaborators (Danabasoglu et al., 2020). The configuration used here, which contributed simulations to CMIP6 (Eyring et al., 2016), represents the coupled climate system at approximately 1° horizontal resolution. The atmospheric component is the Community Atmosphere Model version 6 (CAM6; Bogenschutz et al., 2018), with 32 vertical levels and a model top near 40 km, coupled to the Parallel Ocean Program version 2 (POP2; Smith et al., 2010; Danabasoglu et al., 2012), the Community Land Model version 5 (CLM5; Lawrence et al., 2019), and the Community Ice Code version 5 (CICE5; Hunke et al., 2015). Aerosols are represented using the four-mode Modal Aerosol Module (MAM4; Liu et al., 2016), and cloud microphysics is represented using the Morrison–Gettelman version 2 scheme (MG2; Gettelman and Morrison, 2015).

The CESM2 simulations analysed here are summarised in Table 1. The all-forcing ensemble (ALL) consists of 100 members spanning 1850–2100, with CMIP6 historical forcing applied from 1850 to 2014 and SSP3–7.0 forcing thereafter (Rodgers et al., 2021; Meinshausen et al., 2020). Ensemble spread is generated using both macro- and micro-initialisation strategies: members are initialised from different years of the preindustrial control simulation, with additional round-off-level perturbations applied to atmospheric potential temperature (Rodgers et al., 2021).

https://doi.org/10.5194/egusphere-2026-5006
Preprint. Discussion started: 31 August 2026

Table 1. Summary of the CESM2 experiments analysed in this study.

Name	Period	No. of members analysed	Description
ALL	1850–2100	10 (50)	All forcings evolving. CMIP6 Historical and SSP3-7.0, but with smoothed BMB
AAER	1850–2050	10 (20)	Only anthropogenic aerosols evolving; other forcings fixed at 1850
GHG	1850–2050	10 (15)	Only greenhouse gases evolving; other forcings fixed at 1850
xAER	1920–2050	10 (10)	All forcings evolving except anthropogenic aerosols, which are kept fixed at 1920s level

A common subset of 10 members is used in the main analysis to ensure consistency across experiments. Numbers in parentheses indicate the full ensemble sizes used in the sensitivity analysis.

The ALL ensemble comprises two 50-member subsets that differ in their prescribed biomass-burning aerosol emissions during 1990–2020. One subset uses the default CMIP6 biomass-burning dataset, which includes satellite-derived emissions and enhanced interannual variability during 1997–2014, whereas the other uses an 11-year running-mean-smoothed dataset designed to reduce artificial discontinuities that can generate rectified climate responses (Fasullo et al., 2022; DeRepentigny et al., 2022). Because the CESM2 single-forcing experiments use the smoothed biomass-burning configuration, we use the corresponding 50-member ALL subset as the baseline for comparison.

The CESM2 single-forcing experiments follow either an "only" or an "all-but-one" experimental design and span 1850–2050 (Table 1). In the greenhouse gas ensemble (GHG), only greenhouse-gas concentrations evolve, while all other forcings are fixed at 1850 values. In the anthropogenic aerosol ensemble (AAER), only anthropogenic aerosol emissions evolve. Here, anthropogenic aerosols include industrial, agricultural, domestic, and transport emissions, while excluding anthropogenic changes in biomass burning (van Marle et al., 2017). In the no-aerosol ensemble (xAER), all forcings evolve except anthropogenic aerosols, which are fixed at 1920 levels.

https://doi.org/10.5194/egusphere-2026-5006
Preprint. Discussion started: 31 August 2026

AAER and ALL−xAER both provide estimates of the anthropogenic aerosol contribution, but they represent fundamentally different experimental frameworks. AAER is an "only" experiment in which aerosol emissions evolve while all other forcings remain fixed at preindustrial levels. By contrast, xAER is an "all-but-one" experiment in which non-aerosol forcings evolve simultaneously. Consequently, the aerosol response inferred from ALL−xAER represents the effect of changing aerosol forcing within an evolving climate state that is also being modified by greenhouse gases and other forcings, whereas AAER represents the aerosol response under a background state in which those other forcings are held fixed. This asymmetry provides the basis for testing whether the two approaches yield dynamically equivalent aerosol responses.

The AAER and xAER ensembles contain 20 and 10 members, respectively (Simpson et al., 2023). To ensure a consistent sampling of internal variability, we use 10 members from each ensemble. Sensitivity tests using all available members (i.e., 50 for ALL, 20 for AAER, 15 for GHG, and 10 for xAER) show that the large-scale patterns and main conclusions remain consistent, with only negligible regional variations in the magnitude and statistical significance of the anomalies (Supplementary Figs. S1 and S2). The conclusions are therefore robust to the use of the larger ALL, AAER, and GHG ensembles, while the xAER response is necessarily constrained by its 10 members. The time evolution of key forcing agents, including CO_2, CH_4, SO_2, BC, and SO_4, is documented in Simpson et al. (2023) (see also Supplementary Fig. S3).

2.2 Definition of aerosol-response estimates

We define the directly simulated aerosol response as the ensemble-mean response in AAER and the residual-based aerosol response as the difference between the all-forcing and no-aerosol ensembles, ALL−xAER. For the latter, corresponding ensemble members are paired before differencing, such that each ALL member is differenced from the xAER member with the same ensemble index. This preserves the common component of internally generated variability and reduces the influence of internal variability on the inferred aerosol response. The difference between the two aerosol-response estimates is then defined as (ALL − xAER) – AAER. A non-zero difference indicates that the diagnosed aerosol response depends on the experimental framework. Such differences may arise from nonlinear interactions between aerosol and other forcing agents and/or from differences in the background climate state in which the aerosol forcing is applied. The physical origin of these differences is examined through the associated circulation, SST, and hydroclimate responses.

2.3 Analysis periods and statistical methods

We analyse boreal summer (June–August, JJA) over 1920–2050, the period common to all experiments. To reduce the influence of internal variability while retaining distinct stages of aerosol forcing evolution, responses are evaluated as differences between 21-year climatological means. Two transitions are considered: an historical transition, 1965–1985 minus 1920–1940, and a future transition, 2030–2050 minus 1965–1985.

https://doi.org/10.5194/egusphere-2026-5006
Preprint. Discussion started: 31 August 2026

The historical transition represents the development of substantial Northern Hemisphere anthropogenic aerosol forcing from an early twentieth-century baseline. The future transition represents the evolution from the late twentieth century to the mid-twenty-first century under SSP3–7.0, during which aerosol forcing declines over Europe and North America but continues to increase over parts of South and East Asia. The latter transition therefore represents a spatial redistribution of aerosol forcing rather than a uniform global decline. Considering the two transitions separately allows the diagnosed aerosol response to be evaluated under substantially different forcing and background climate states, without conflating the mechanisms operating during the historical aerosol increase with those associated with the subsequent redistribution of aerosol forcing in the cumulative 1920–2050 change.

For each ensemble member, JJA climatological means are first calculated for each 21-year period, and the difference between periods is then computed for each member. Ensemble-mean responses are subsequently calculated across members. For the ALL−xAER estimate, the corresponding member-by-member differences are calculated before averaging across the paired ensemble. The directly simulated AAER response is calculated from the corresponding member-by-member differences within the AAER ensemble.

Statistical significance of the ensemble-mean responses is assessed using a two-sided Student's t-test based on inter-member variability, with significance defined at the 95% confidence level. For the paired ALL−xAER estimate, the test is applied to the distribution of member-paired differences. Statistical significance of the difference between the two aerosol-response estimates is assessed from the corresponding distributions of these individual differences.

Robustness is additionally evaluated using ensemble agreement, defined as the fraction of ensemble members exhibiting the same sign as the ensemble-mean change. In spatial maps, regions where at least 95% of ensemble members agree on the sign of the change are stippled.

3 Results

3.1 Surface climate

Figure 1a–b shows the spatial distribution of JJA-mean land SO_2 emission changes for the two selected transitions, used here as a proxy for the broader anthropogenic aerosol changes prescribed in the CESM2 experiments. During 1965–1985 relative to 1920–1940, SO_2 emissions increase across the major Northern Hemisphere industrial regions, particularly Europe, North America, and East Asia. In contrast, during 2030–2050 relative to 1965–1985, emissions decline substantially over Europe and North America but continue to increase over South and East Asia. The two transitions therefore represent contrasting stages of the anthropogenic aerosol evolution: an historical intensification of Northern Hemisphere aerosol emissions followed by a post-peak decline and subsequent plateau in global SO_2 emissions, accompanied by a pronounced geographical redistribution of emissions. Importantly, contrasting regional trends result in a slower post-peak decline in global SO_2 emissions, such that emissions at the end of the period remain substantially higher than in 1940 (Lund et al., 2019; Turnock et al., 2020).

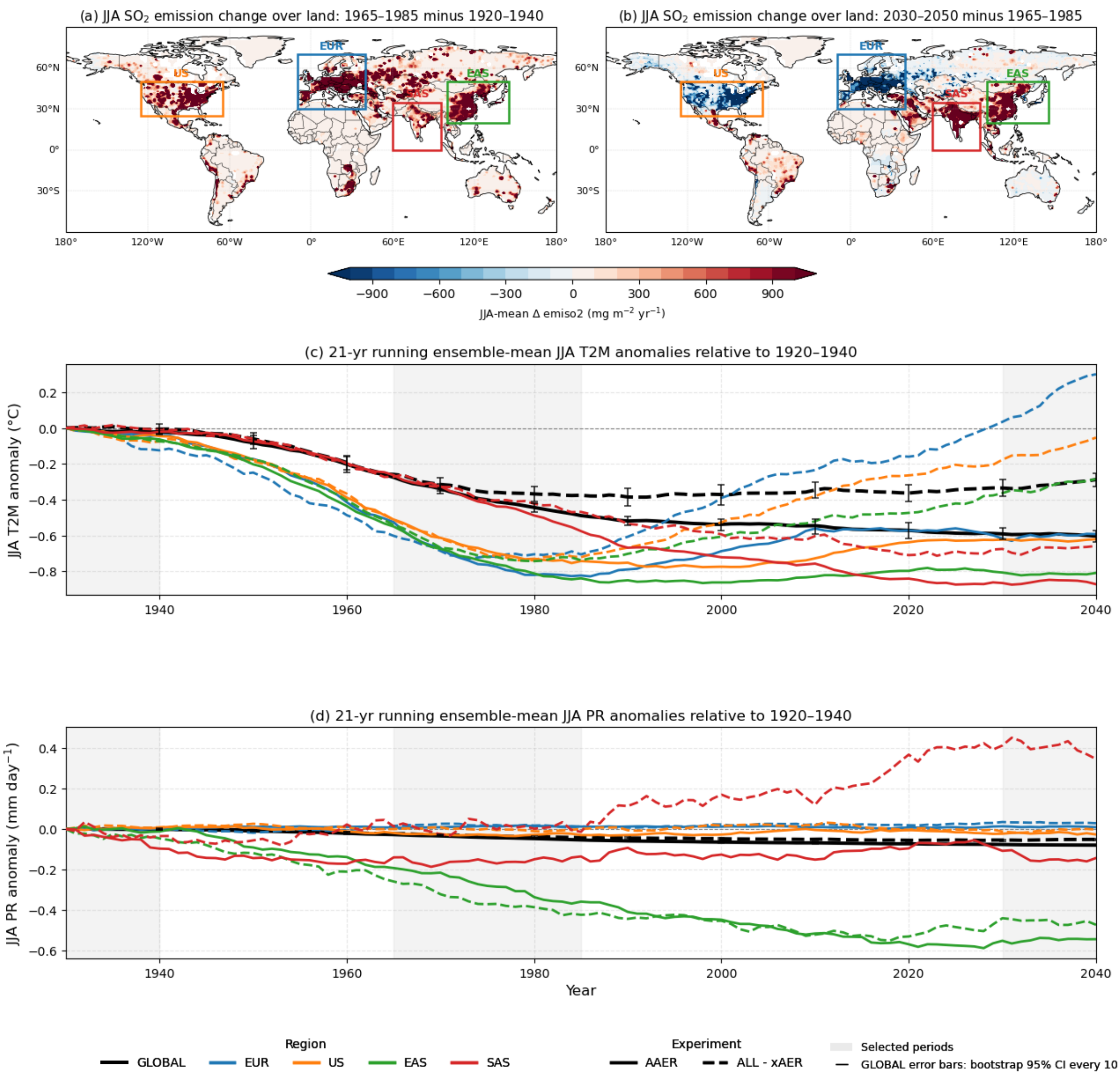

Figure 1. Spatial distribution of land SO_2 emission changes and temporal variations of regional climate responses (a) and (b) during JJA: SO_2 emission changes over land for 1965–1985 relative to 1920–1940 and for 2030–2050 relative to 1965–1985, respectively. Boxes indicate the four selected regions used in the regional time-series analysis: Europe (EUR), United States/North America (US), East Asia (EAS), and South Asia (SAS). Panels (c) and (d) show 21-year running mean anomalies relative to 1920–1940 for 2-m air temperature (T2M; °C) and precipitation (PR; mm day^{-1}), respectively. Solid lines denote the aerosol-only response from AAER, while dashed lines denote the aerosol contribution inferred from ALL − xAER.

https://doi.org/10.5194/egusphere-2026-5006
Preprint. Discussion started: 31 August 2026

The regional time series of JJA near-surface (2-m) air temperature and precipitation anomalies (Fig. 1c–d), averaged over the major emission-source regions shown in Fig. 1a–b and compared with the global land mean, illustrate the contrasting evolution of aerosol-related climate responses. Under AAER, temperature anomalies become progressively more negative until approximately the 1980s, consistent with the increasing aerosol forcing in the absence of evolving non-aerosol forcings. Cooling is strongest over Europe, the US, and East Asia, whereas the response over South Asia develops more gradually. Thereafter, anomalies over Europe and the US decrease, especially and faster over Europe, to then fluctuate around a persistent negative value through the mid-twenty-first century. East Asian anomalies undergo small oscillations around the negative peak in the early 2000s, while South Asia continues to cool, resulting in the coldest region by the end of the record.

The ALL−xAER response evolves differently. Cooling again develops through the late twentieth century, but the subsequent response is more transient and regionally heterogeneous. As aerosol emissions decline over Europe and North America, the temperature response over Europe reverses from cooling to warming, reaching approximately +0.3°C by 2040. The US and East Asia also warm relative to their late-century minima but remain cooler than their early-period values, whereas South Asia continues to cool, broadly following the evolution in AAER but with a somewhat smaller amplitude. A similar divergence is evident in the global land mean. Thus, while the two approaches produce broadly comparable temperature responses during the historical transition, their trajectories increasingly diverge as the background climate evolves and aerosol forcing becomes spatially redistributed.

The regional precipitation time series show an even stronger dependence on the diagnosed aerosol response (Fig. 1d). East Asia exhibits the most persistent drying in both experiments, reaching approximately −0.5 to −0.6 mm day^{-1} by 2040. Over South Asia, however, the two responses diverge markedly. In AAER, precipitation decreases through the historical period and subsequently remains slightly below its early-period level. The ALL−xAER response initially shows a similar tendency but reverses towards wetter conditions from approximately the 1990s onward, reaching about +0.45 mm day^{-1} by 2040. Changes over Europe and North America are comparatively small in the regional mean. These contrasting trajectories, particularly over South Asia and East Asia, motivate examination of the spatial precipitation and circulation responses below.

The spatial distribution of the JJA mean 2-m air temperature response further illustrates the evolution from approximate agreement to pronounced divergence between the two approaches (Fig. 2). During 1965–1985 relative to 1920–1940, both AAER and ALL−xAER produce widespread Northern Hemisphere cooling, particularly across Eurasia and northern North America (Figs. 2a–b). This pattern is consistent with the increase in aerosol forcing and associated reductions in surface shortwave radiation over major source regions. The difference between the two estimates is comparatively weak and is not statistically significant over most regions (Fig. 2c), indicating that the two experimental approaches provide broadly consistent estimates of the historical aerosol-induced temperature response. Some regional differences are nevertheless apparent,

https://doi.org/10.5194/egusphere-2026-5006
Preprint. Discussion started: 31 August 2026

including stronger cooling in ALL−xAER over central Europe, northern Asia, and North America, and weaker cooling over northern Europe and the northwestern Pacific.

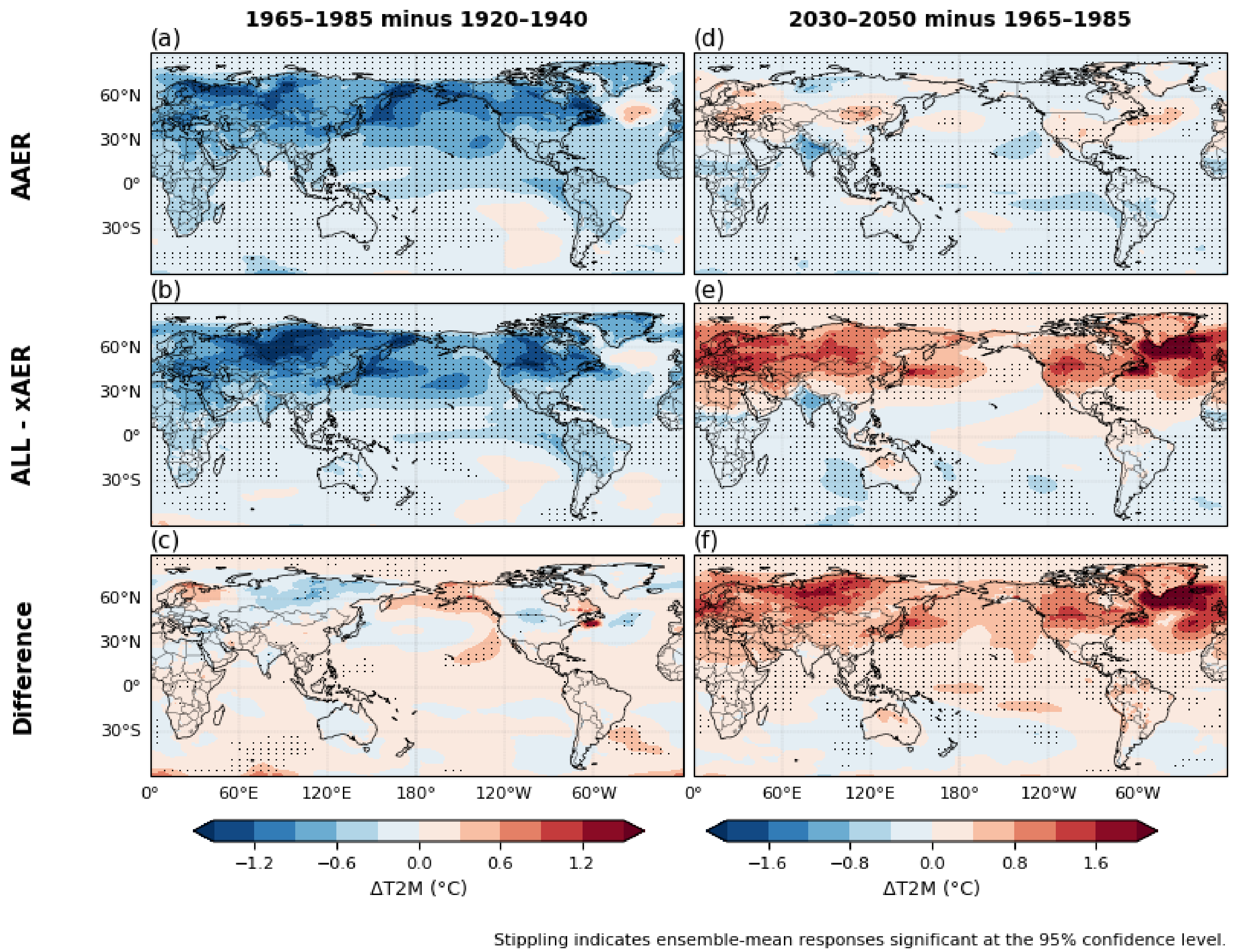

Figure 2. Difference in JJA mean near-surface air temperature (ΔT2M, °C) between two different periods: 1965–1985 relative to 1920–1940 (left) and 2030–2050 relative to 1965–1985 (right). (a), (d) AAER, (b), (e) ALL−xAER, and (c), (f) the difference between them (ALL−xAER minus AAER). Stippling indicates anomalies that are statistically significant at the 95% confidence level.

During 2030–2050 relative to 1965–1985, the contrast between the two approaches becomes much more pronounced (Figs. 2d–f). Both experiments show warming across much of the Northern Hemisphere midlatitudes, consistent with declining aerosol forcing over Europe and North America, while continued increases in Asian aerosol emissions contribute to regional cooling, particularly in AAER. The warming in ALL−xAER is substantially stronger than in AAER over much of the globe, with the largest differences occurring across Northern Hemisphere mid- and high-latitude land regions, including Europe,

https://doi.org/10.5194/egusphere-2026-5006
Preprint. Discussion started: 31 August 2026

northern Asia, and North America (Fig. 2f). Differences extend over adjacent ocean regions, most notably the subpolar North Atlantic. The spatially coherent nature of these differences contrasts sharply with the relatively small historical discrepancy and indicates that the equivalence between direct and residual-based aerosol estimates breaks down under the future climate state.

The JJA precipitation responses exhibit considerably greater spatial complexity than the temperature responses (Fig. 3). During 1965–1985 relative to 1920–1940, AAER and ALL−xAER share several broad features, but substantial regional differences are already apparent over the Asian monsoon region and tropical Indo-Pacific (Figs. 3a–c). The largest precipitation responses occur over regions of strong climatological rainfall, including the Indo-Pacific warm pool, South Asia, and the Maritime Continent. Both experiments produce drying over East and Southeast Asia, consistent with increasing aerosol forcing over these regions, although the drying is generally stronger and more spatially extensive in ALL−xAER. Over South Asia, the responses differ more markedly: ALL−xAER produces widespread wetting across the Indian subcontinent, whereas AAER exhibits a weaker and more heterogeneous response, including modest drying over parts of southern India.

https://doi.org/10.5194/egusphere-2026-5006
Preprint. Discussion started: 31 August 2026

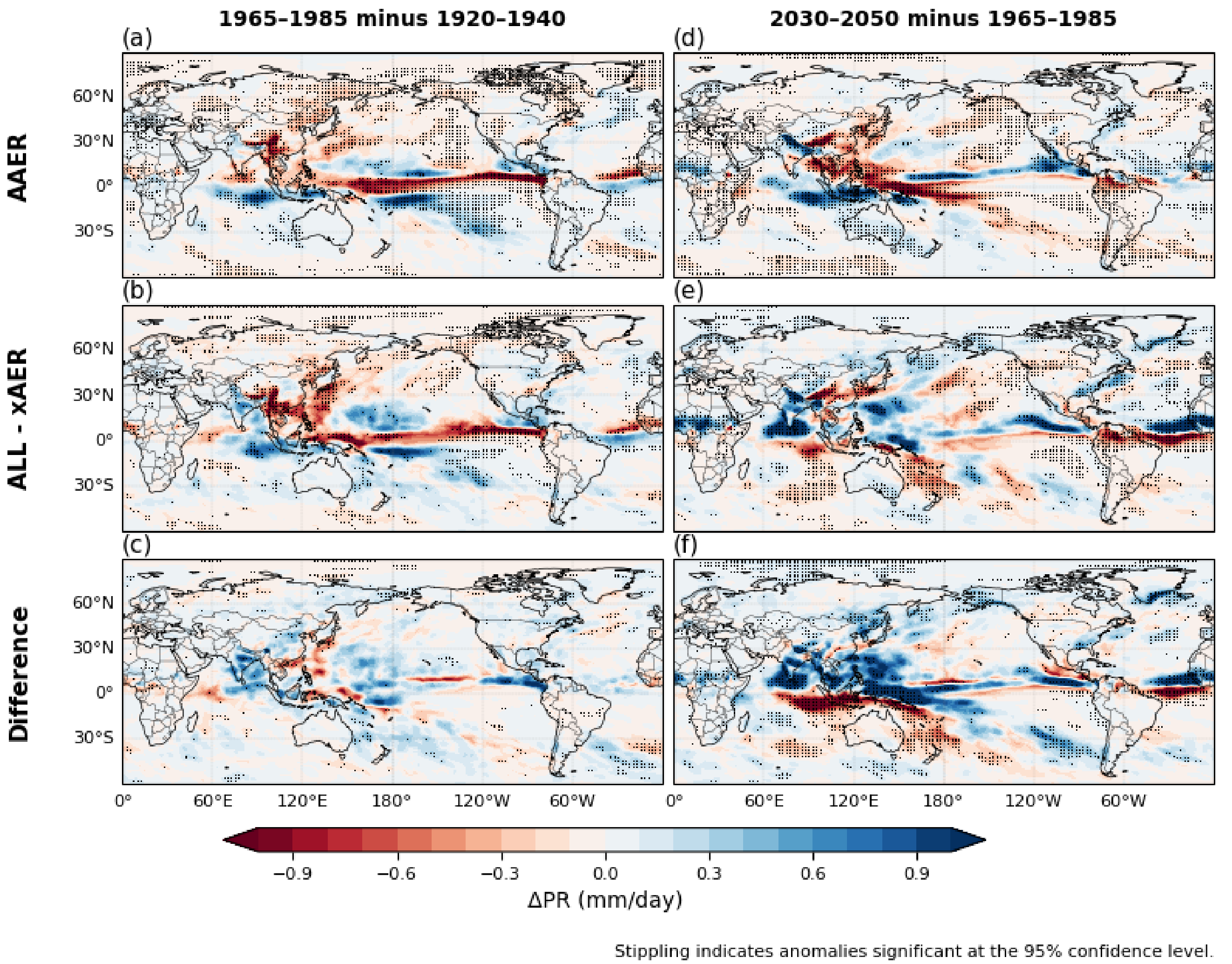

285 **Figure 3. Difference in JJA mean precipitation (Δpr; mm day⁻¹) between two different periods: 1965–1985 relative to 1920–1940 (left) and 2030–2050 relative to 1965–1985 (right). (a), (d) AAER, (b), (e) ALL−xAER, and (c), (f) the difference between them (ALL−xAER minus AAER). Stippling indicates anomalies that are statistically significant at the 95% confidence level.**

The tropical precipitation response in this historical transition also indicates a broader reorganisation of convection. In both experiments, particularly AAER, enhanced precipitation extends westward from the Maritime Continent towards the eastern Indian Ocean, accompanied by a southward displacement of the Pacific ITCZ and significant off-equatorial precipitation anomalies. Over Africa and the tropical Atlantic, both simulations exhibit a southward displacement of the monsoon rainfall maximum, with drying to the north and increased rainfall to the south, although these changes are generally stronger in ALL−xAER. The difference field therefore reflects not simply a difference in the magnitude of the aerosol response but a redistribution of precipitation anomalies across tropical and extratropical regions. Percentage-change maps (Fig. S4, left

https://doi.org/10.5194/egusphere-2026-5006
Preprint. Discussion started: 31 August 2026

column) further highlight differences over regions of relatively low climatological precipitation. Over western Europe and the Mediterranean, for example, AAER produces increased precipitation whereas ALL−xAER shifts the positive response eastward, generating a zonal dipole in the difference field. Similarly, stronger drying in AAER over parts of Eurasia produces a positive difference, while enhanced wetting in ALL−xAER over Australia is associated with changes in the tropical precipitation pattern.

The divergence between the two aerosol-response estimates becomes substantially larger and more spatially coherent during 2030–2050 relative to 1965–1985 (Figs. 3d–f). AAER produces widespread drying across East and Southeast Asia extending into the Maritime Continent (Fig. 3d), consistent with the continued increase in Asian aerosol emissions. In contrast, ALL−xAER shows considerably weaker continental drying and increased precipitation over parts of the Maritime Continent and South Asia (Fig. 3e). The resulting difference field is characterised by pronounced positive precipitation anomalies across East Asia, Southeast Asia, and the Maritime Continent, with localised negative anomalies primarily south of the equator (Fig. 3f). The divergence over South Asia is particularly pronounced, with wetting strengthening in ALL−xAER while the AAER response remains weak and spatially heterogeneous.

Differences also extend throughout the tropical Indo-Pacific. In AAER, precipitation changes during the future transition are concentrated over the eastern Indian Ocean, Maritime Continent, and western Pacific, indicating a broad reorganisation of tropical convection rather than a simple westward displacement of rainfall. ALL−xAER exhibits a different spatial structure, with enhanced precipitation over parts of the Indian Ocean and western Pacific but drying over the southern Maritime Continent. Outside the Indo-Pacific, both experiments show a meridional precipitation dipole associated with a northward displacement of the West African monsoon/Sahel rainfall belt, although the displacement is stronger in ALL−xAER. Percentage-change maps (Fig. S4, right column) reveal additional differences across the extratropics. Over Europe and the Mediterranean, AAER changes from wetting in the historical transition to drying in the future transition, whereas ALL−xAER maintains predominantly positive precipitation anomalies, producing a widespread positive difference.

Overall, the surface climate responses reveal a clear transition from broad agreement between AAER and ALL−xAER during the historical aerosol increase to substantial and spatially coherent divergence during the future transition. The divergence is particularly pronounced for precipitation and involves coordinated changes across the Asian monsoon region, tropical Indo-Pacific, African monsoon, and Northern Hemisphere extratropics. The spatial complexity of these differences indicates that they cannot be interpreted simply as an amplification or attenuation of the directly simulated aerosol response. Instead, the contrasting patterns point to a reorganisation of the underlying circulation and moisture-transport pathways, which are examined in the following sections.

https://doi.org/10.5194/egusphere-2026-5006
Preprint. Discussion started: 31 August 2026

The spatial patterns of both temperature and precipitation responses, including the differences between AAER and ALL−xAER, are broadly consistent when using the full available ensemble means rather than the 10-member ensembles adopted for the main analysis, with only modest regional differences in magnitude (Figs. S1 and S2).

3.2 Low-tropospheric circulation and moisture transport changes

To place the surface temperature and precipitation responses described above into their dynamical context, we examine sea-level pressure (SLP) and 850-hPa wind anomalies (Fig. 4), together with vertically integrated water vapour transport and moisture-flux convergence (Fig. 5).

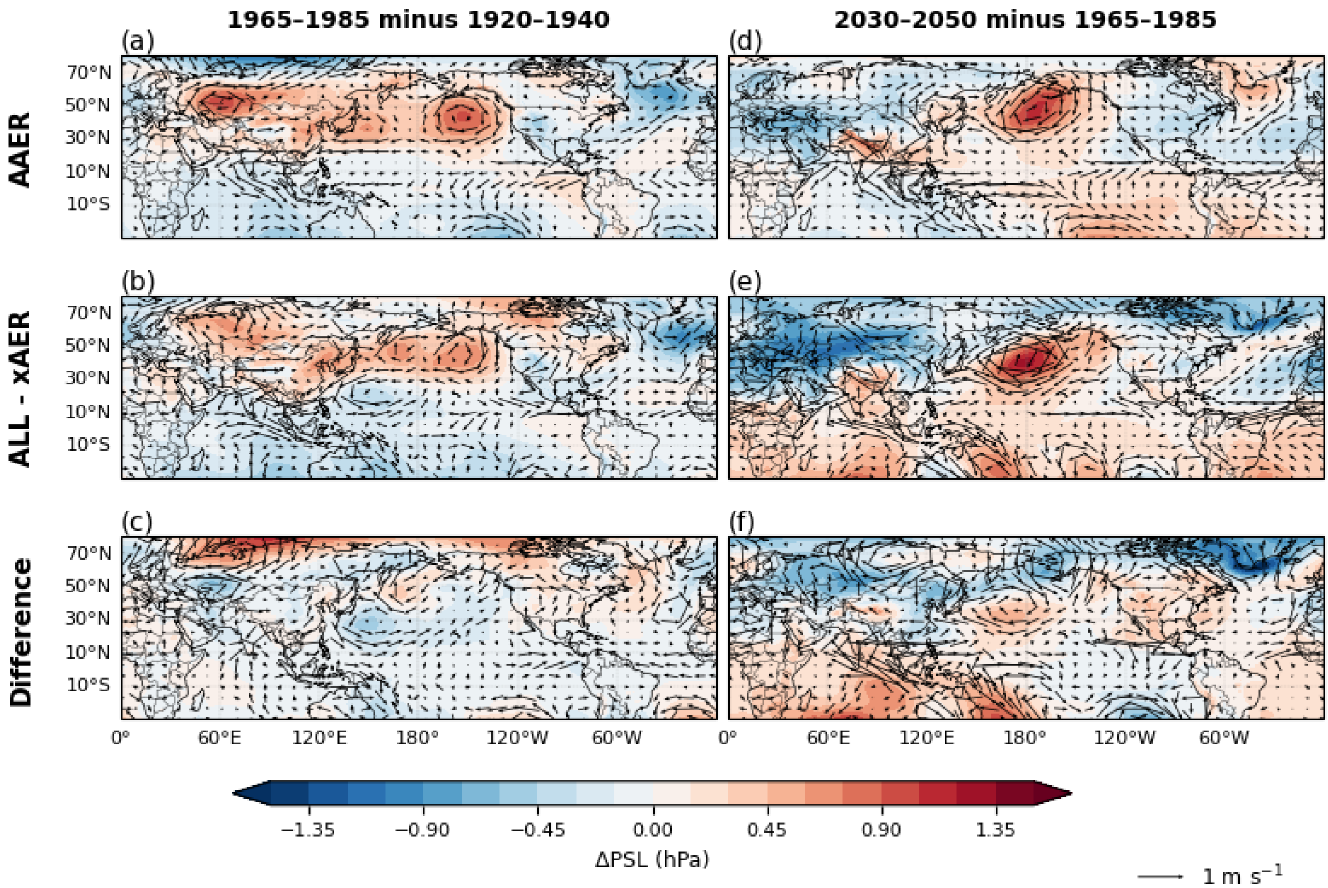

Figure 4. Changes in JJA mean sea level pressure (shading, unit: hPa) and wind (vector, unit: m s^{-1}) at 850 hPa between two different periods: 1965–1985 relative to 1920–1940 (left) and 2030–2050 relative to 1965–1985 (right) for the (a), (d) AAER, (b), (e) ALL−xAER, and (c), (f) the difference between them (ALL−xAER minus AAER).

https://doi.org/10.5194/egusphere-2026-5006
Preprint. Discussion started: 31 August 2026

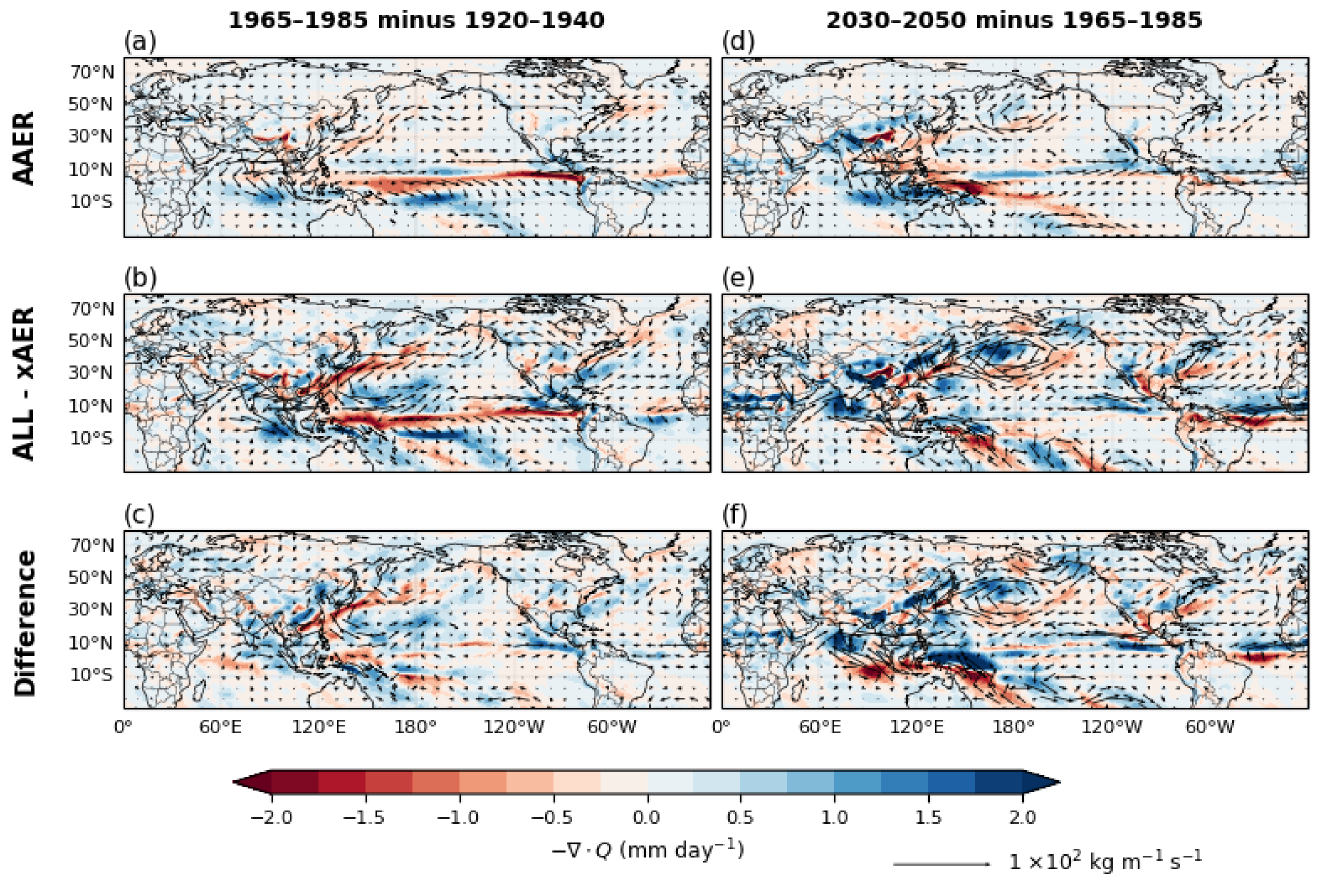

Figure 5. Changes in JJA mean vertically integrated water vapor transport vectors (unit: 10^2 kg m^{-1} s^{-1}) and moisture flux convergence (shading, unit: mm day^{-1}) in two different periods: 1965–1985 relative to 1920–1940 (left) and 2030–2050 relative to 1965–1985 (right) for (a), (d) AAER, (b), (e) ALL−xAER, and (c), (f) the difference between them (ALL−xAER minus AAER).

During 1965–1985 relative to 1920–1940, AAER and ALL−xAER produce broadly similar large-scale circulation responses across the Northern Hemisphere (Figs. 4a, b and 5a, b). Positive SLP anomalies dominate the Northern Hemisphere midlatitudes, consistent with the widespread surface cooling associated with increasing aerosol loading (Fig. 2a, b). The response, however, is strongly modulated by regional action centres rather than representing a zonally uniform adjustment. These alternating anticyclonic and cyclonic centres determine the regional redistribution of moisture and provide the dynamical framework for the precipitation responses discussed in Sect. 3.1.

Over the North Atlantic, a cyclonic anomaly promotes enhanced southwesterly flow towards western Europe, increasing onshore moisture transport and contributing to the wetting response over the region in both experiments (Figs. 3a, b, 4a, b and 5a, b). Across northern Eurasia, broad positive SLP anomalies generate anomalous northerly flow along their eastern flank, favouring the transport of colder and drier continental air. This circulation is consistent with the widespread cooling and drying

https://doi.org/10.5194/egusphere-2026-5006
Preprint. Discussion started: 31 August 2026

over northeastern Asia, which are somewhat stronger in AAER than in ALL−xAER. Farther southeast, a positive SLP anomaly over eastern China and the western North Pacific weakens the climatological southwesterly monsoon flow into China and Indochina, producing moisture divergence and reduced precipitation. At the same time, anomalous easterlies over the tropical western Pacific oppose the climatological monsoon inflow into India while transporting moisture westward towards the Indian subcontinent. This moisture converges over India, particularly in ALL−xAER, where anomalous westerlies over the northern Arabian Sea associated with the thermally induced cyclonic circulation over Afghanistan and Pakistan further enhance the moisture supply (Figs. 4a, b and 5a, b). This circulation configuration is consistent with the widespread wetting across much of India.

Over the tropical Indo-Pacific, both experiments exhibit a pronounced band of moisture divergence across the equatorial western Pacific (Fig. 5a, b), indicative of suppressed convection and consistent with the negative precipitation anomalies over the equatorial Pacific (Fig. 3a, b). This response is associated with broader adjustments of the tropical Walker circulation. Over western Africa and the tropical Atlantic, anomalous anticyclonic low-level flow inhibits the northward migration of the monsoon rainband, producing moisture divergence north of the climatological rainfall maximum and convergence to the south. The resulting meridional redistribution of moisture is consistent with the southward displacement of the West African monsoon. Over North America, an anomalous anticyclone over the northeastern Pacific, together with weaker cyclonic anomalies over the southern United States, favours the advection of cooler and drier air along the Pacific coast and reduces westerly moisture transport into the western United States, broadly consistent with the regional drying response (Figs. 3a, b, 5a, b and S4a, b).

Thus, despite the broadly similar surface climate responses, the two experiments already exhibit differences in the spatial organisation of the low-level circulation. The SLP action centres are generally stronger but more spatially confined in AAER, whereas ALL−xAER exhibits weaker but more spatially extensive anomalies. The resulting difference field (Fig. 4c) contains alternating centres of action across the Northern Hemisphere extratropics, indicating that the discrepancy between the two aerosol-response estimates reflects differences in circulation structure rather than simply a uniform difference in amplitude. These dynamical differences are relatively modest during the historical transition but provide an early indication that the two experimental frameworks do not produce identical responses.

During 2030–2050 relative to 1965–1985, the circulation response changes substantially in both experiments, while the contrast between AAER and ALL−xAER becomes much more pronounced (Figs. 4d–f and 5d–f). In AAER, the positive SLP anomalies that characterised the Northern Hemisphere midlatitudes during the historical transition largely reverse, producing widespread negative anomalies over Europe and the Mediterranean and a weaker negative centre over North America. In contrast, the positive anomaly over the North Pacific strengthens and becomes the dominant extratropical feature (Fig. 4d). Over the Asian monsoon region, anticyclonic flow over Indochina and northern India remains consistent with continued drying across East and Southeast Asia, where precipitation decreases locally by approximately 10–20% of the climatological mean

https://doi.org/10.5194/egusphere-2026-5006
Preprint. Discussion started: 31 August 2026

(Figs. 3d and S4d). Positive SLP anomalies over South Asia continue to constrain the cross-equatorial monsoon inflow, although moisture transported from the western Pacific still produces convergence over northern India and localised wetting (Figs. 3d–e, 4d and 5d). The band of moisture divergence over the equatorial western Pacific also persists, indicating that the broad tropical circulation response remains similar to that during the historical transition.

The ALL−xAER circulation response is markedly different. Negative SLP anomalies become stronger and more spatially extensive, extending from the North Atlantic across Europe into northern Eurasia. This configuration is consistent with the warmer background climate associated with the simultaneous evolution of greenhouse gases and other non-aerosol forcings in the ALL−xAER estimate. The positive North Pacific anomaly is also stronger than in AAER. Most notably, a pronounced negative SLP centre develops over East Asia near 30°–40°N (Fig. 4e), with no comparable feature in AAER. This low-pressure anomaly is accompanied by substantial surface warming and represents a major reorganisation of the circulation over East Asia. It is associated with a strong anomalous southwesterly moisture-transport pathway extending from the Arabian Sea across India and into East Asia (Fig. 5e). The resulting moisture convergence spans the Indian subcontinent, Southeast Asia, and eastern China, producing a substantially wetter and more spatially coherent precipitation response than in AAER (Figs. 3e and S4e).

The contrast in moisture transport is particularly striking across the Indo-Pacific sector. In AAER, anomalous moisture transport remains relatively fragmented, with moisture divergence over parts of the tropical western Pacific and circulation anomalies that limit the monsoon inflow across South and East Asia. In ALL−xAER, by contrast, the anomalous southwesterly flow forms a more continuous pathway from the Arabian Sea across the Asian monsoon region towards East Asia, accompanied by widespread moisture convergence. The difference between the two experiments therefore represents not merely a change in the magnitude of moisture transport but a reorganisation of the pathway through which moisture is supplied to the Asian monsoon region.

These results show that the increasing divergence between AAER and ALL−xAER during the future transition has a clear dynamical origin. Whereas the historical responses share a broadly similar circulation structure, the future responses develop substantially different SLP patterns and moisture-transport pathways, particularly across the North Atlantic–Eurasian sector and the Indo-Pacific. The resulting circulation reorganisation provides a dynamical explanation for the contrasting regional precipitation responses and indicates that the future discrepancy between the two aerosol-response estimates is not simply a local thermodynamic consequence of changing aerosol emissions. In the following section, we show that these low-level circulation differences are accompanied by changes in upper-tropospheric flow and Rossby-wave propagation, providing a broader hemispheric dynamical framework for the divergent hydroclimate responses.

https://doi.org/10.5194/egusphere-2026-5006
Preprint. Discussion started: 31 August 2026

3.3 Upper-tropospheric circulation and wave propagation

To further examine the large-scale dynamical setting, we analyse upper-tropospheric zonal wind (Fig. 6), streamfunction and wave activity flux (WAF; Fig. 7). The zonal wind response characterises changes in the position and strength of the principal upper-tropospheric jets, while the streamfunction reveals the associated large-scale wave structure. The WAF, calculated following Takaya and Nakamura (2001), provides a phase-independent diagnostic of quasi-geostrophic Rossby-wave propagation on a zonally varying background flow. Because the WAF depends on both the perturbation streamfunction and the background wind, it identifies the pathways along which Rossby-wave activity is preferentially guided by the upper-tropospheric jet. To further characterise the tropical circulation and identify potential sources of the extratropical wave response, we also analyse the linearised Rossby wave source (RWS; Fig. 8) and the divergent circulation (Fig. 9). The RWS diagnoses the generation of Rossby-wave activity associated with the interaction between divergent flow and absolute vorticity and therefore provides a dynamical link between anomalous tropical convection and extratropical wave responses.

https://doi.org/10.5194/egusphere-2026-5006
Preprint. Discussion started: 31 August 2026

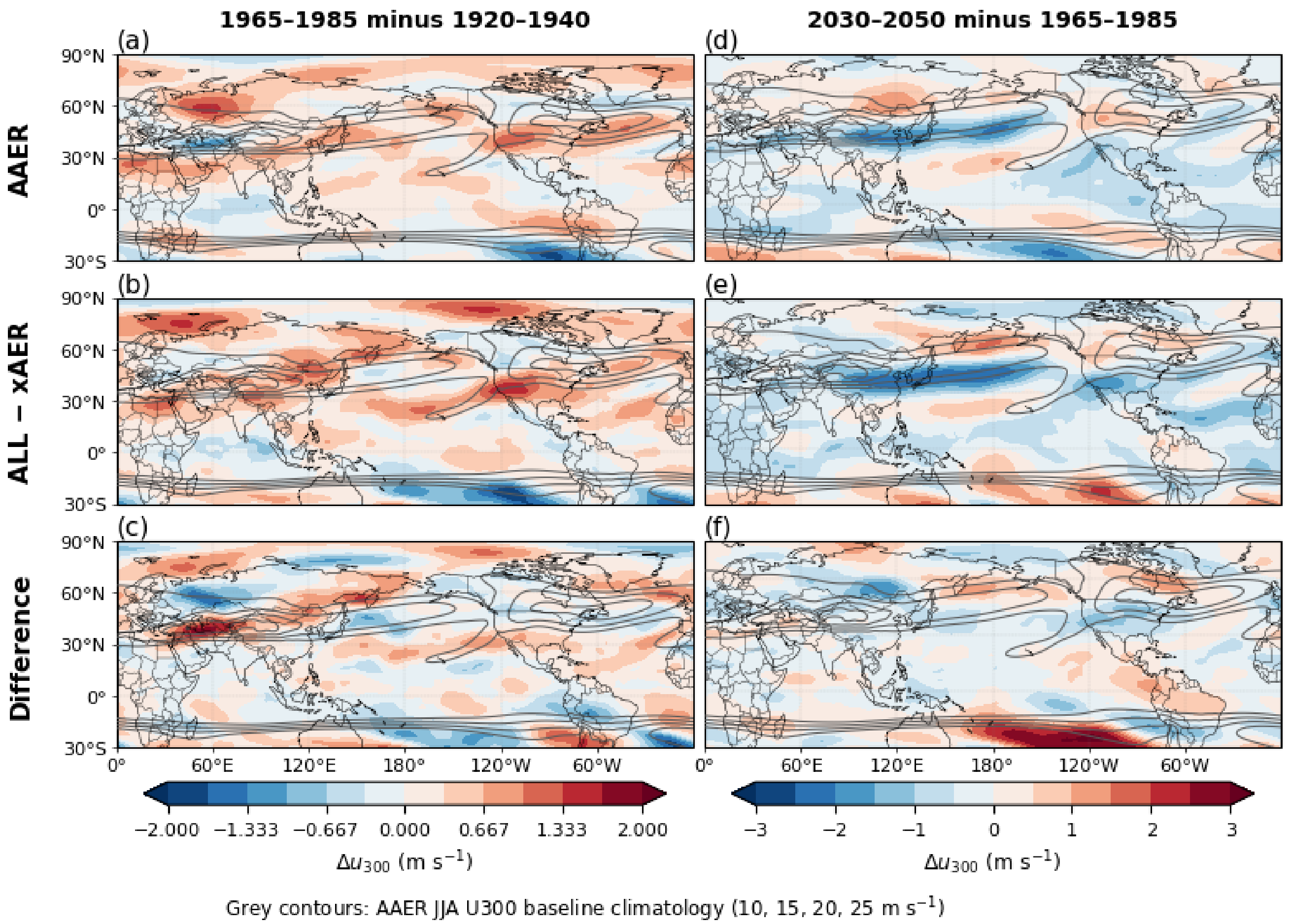

Figure 6. Changes in JJA mean zonal wind at 300 hPa (shading, unit: m s⁻¹) between two different periods: 1965–1985 relative to 1920–1940 (left) and 2030–2050 relative to 1965–1985 (right) for the (a), (d) AAER, (b), (e) ALL−xAER, and (c), (f) difference between them (ALL−xAER minus AAER). Grey contours show the AAER JJA mean 300-hPa zonal-wind climatology for the corresponding baseline period (1920–1940 for the left column and 1965–1985 for the right column), with contour levels of 10, 15, 20, and 25 m s⁻¹.

https://doi.org/10.5194/egusphere-2026-5006
Preprint. Discussion started: 31 August 2026

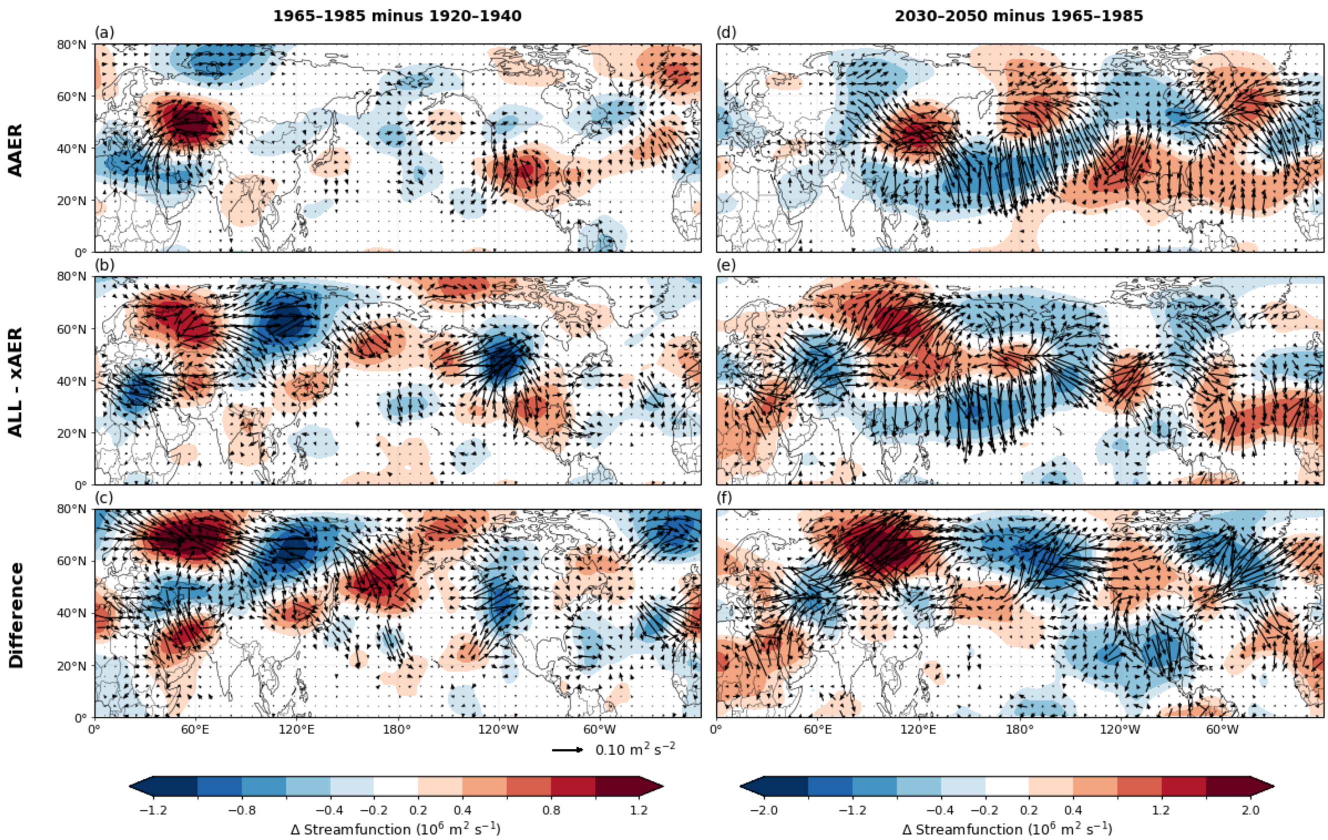

445 **Figure 7. Changes in JJA mean wave activity flux (vector, unit: $m^2\ s^{-2}$) and stream function (shading, unit: $10^6\ m^2\ s^{-1}$) in two different periods: 1965–1985 relative to 1920–1940 (left) and 2030–2050 relative to 1965–1985 (right) for the (a), (d) AAER, (b), (e) ALL−xAER, and (c), (f) the difference between them (ALL−xAER minus AAER).**

https://doi.org/10.5194/egusphere-2026-5006
Preprint. Discussion started: 31 August 2026

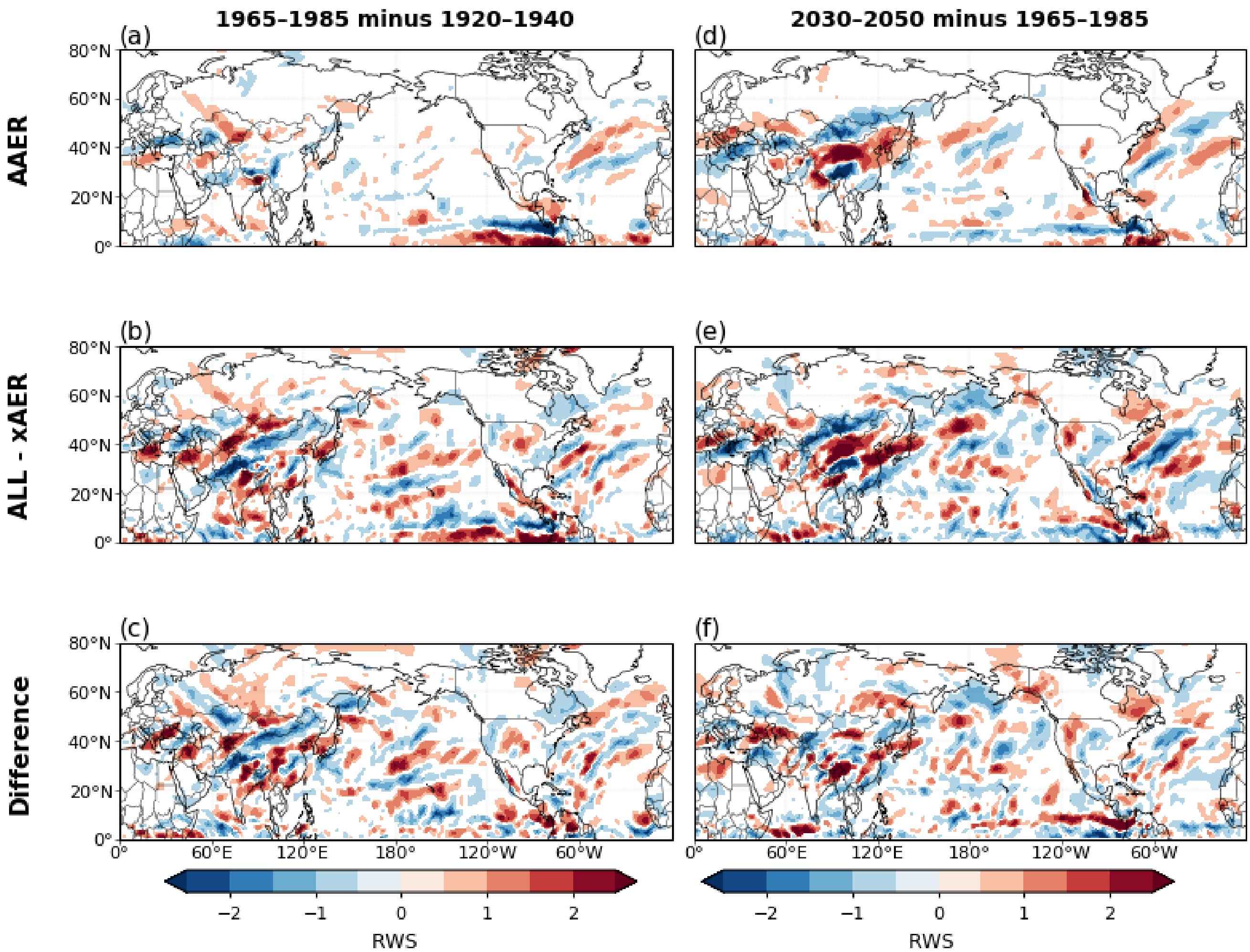

450 **Figure 8. Changes in JJA 200-hPa linearised Rossby wave source (RWS; shading, 10^{-11} s^{-2}) for 1965–1985 relative to 1920–1940 (left) and 2030–2050 relative to 1965–1985 (right), for (a, d) AAER, (b, e) ALL−xAER, and (c, f) the difference between them (ALL−xAER minus AAER). Weak RWS anomalies with absolute magnitudes smaller than 0.5×10^{-11} s^{-2} are masked in white to highlight the stronger RWS responses.**

https://doi.org/10.5194/egusphere-2026-5006
Preprint. Discussion started: 31 August 2026

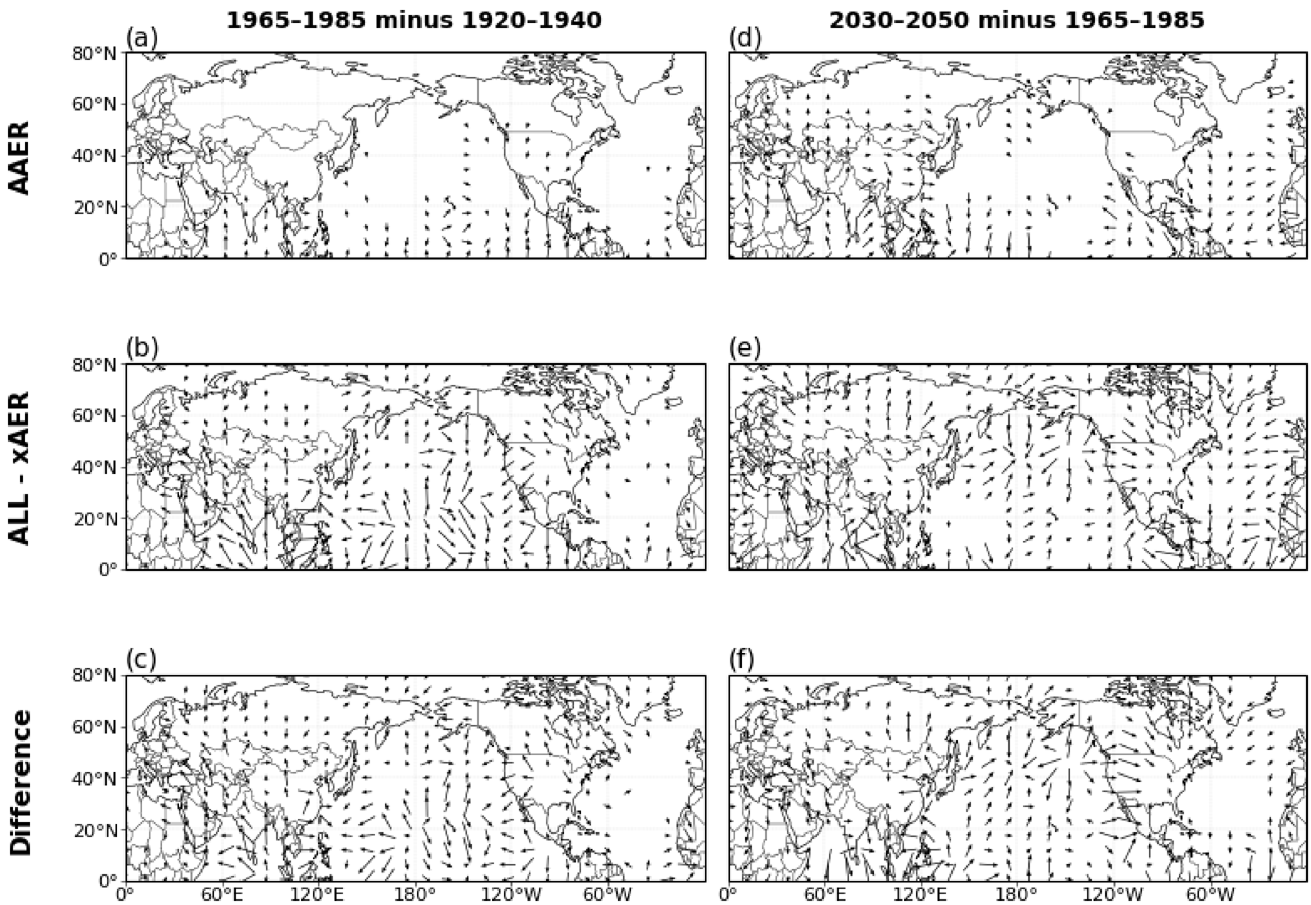

455 **Figure 9. Changes in JJA 200-hPa divergent wind response (vectors, m s^{-1}) for 1965–1985 relative to 1920–1940 (left) and 2030–2050 relative to 1965–1985 (right), for (a, d) AAER, (b, e) ALL−xAER, and (c, f) the difference between them (ALL−xAER minus AAER). Vectors with magnitudes smaller than 0.10 m s^{-1} are omitted for clarity. The reference vector denotes 0.5 m s^{-1}.**

During 1965–1985 relative to 1920–1940, AAER produces negative zonal-wind anomalies along the northern flank of the North Atlantic jet core, indicating a southward displacement of the Atlantic jet (Fig. 6a). This response is consistent with aerosol-induced cooling over Europe and North America reducing the meridional temperature gradient and hence the thermal-wind support for the upper-tropospheric jet. Over the Pacific, the response is more spatially complex, with weakened westerlies over the western and central jet core and strengthened westerlies towards the eastern Pacific exit region, indicative of an eastward extension of the Pacific jet.

ALL−xAER shares some of these features, including weakening and southward displacement of the jets in their entrance and core regions, but also exhibits important differences (Fig. 6b). In particular, strengthening and northeastward extension of the jets over their core and exit regions are evident, consistent with the superposition of the circulation response to greenhouse-gas forcing (Fig. S5a; e.g., Grise and Polvani, 2014). The resulting difference field (Fig. 6c) is characterised by enhanced westerlies along the Asian jet, a more poleward Pacific jet, and a corresponding poleward displacement of the North Atlantic jet. Thus, even during the historical transition, the residual-based estimate contains a substantial modification of the aerosol-driven jet response associated with the evolving non-aerosol-forced background state.

The upper-tropospheric streamfunction responses show a corresponding hemispheric wave structure (Fig. 7a,b). Both experiments exhibit alternating positive and negative anomalies across the Northern Hemisphere midlatitudes, broadly resembling a quasi-stationary Rossby-wave train with zonal wavenumber 4–5. The wave pattern is particularly pronounced in ALL−xAER, although a weaker but coherent structure is also present in AAER. The associated meridional wind anomalies (Fig. S6a–c) provide a complementary representation of this wave pattern by more clearly resolving the alternating northerly and southerly flow associated with the wave train. WAF vectors indicate predominantly eastward propagation, consistent with the upper-tropospheric jet acting as the principal waveguide.

In AAER, wave activity is strongest over the Mediterranean and central Asian sector, from where it propagates northeastward towards a pronounced anticyclonic anomaly over northeastern Europe. Downstream propagation across Eurasia is comparatively weak but remains discernible, with the signal extending towards North America where it becomes more pronounced. A secondary pathway extends from northeastern Canada towards the Arctic. In ALL−xAER, the principal action centres remain broadly similar, but the streamfunction anomalies are stronger and the WAF pathway is more coherent and displaced poleward. Enhanced wave activity extends from northern Europe across Eurasia, consistent with the more poleward position of the upper-tropospheric jet. The modified jet waveguide therefore favours a different spatial organisation and more efficient downstream propagation of Rossby-wave activity.

https://doi.org/10.5194/egusphere-2026-5006
Preprint. Discussion started: 31 August 2026

The divergent circulation and RWS provide further insight into the tropical contribution to this wave response (Figs. 8a–c and 9a–c). Over South Asia, anomalous upper-level divergence associated with enhanced monsoon convection contributes to a pronounced positive RWS anomaly through its interaction with the background absolute-vorticity field. Weak northeastward WAF propagation from central China is evident in both experiments but is more coherent in ALL−xAER. This correspondence suggests that diabatically forced Rossby-wave activity generated over South Asia contributes to the downstream circulation anomalies, although the relative contributions of individual aerosol source regions cannot be isolated from these experiments.

The upper-level wave response is also dynamically connected to the lower-tropospheric circulation. The large anticyclonic anomaly over northeastern Europe in AAER has a coherent vertical structure, with corresponding surface cyclonic and anticyclonic anomalies on its western and eastern flanks, respectively. A similar vertical organisation is evident over the northeastern Pacific. Mid-tropospheric vertical velocity anomalies (Fig. S7a–c) display comparable wave-like structures, providing further evidence of a vertically coherent circulation response. The interaction between aerosol and non-aerosol forcing is particularly apparent over western Europe, where changes in the low-level pressure and wind fields are consistent with the secondary circulation associated with the displaced upper-level jet.

These upper-tropospheric differences provide an important dynamical context for the precipitation differences identified in Sect. 3.1. In the ALL−xAER minus AAER response, the streamfunction, vertical velocity, and divergent circulation anomalies broadly correspond to the regional precipitation anomalies, indicating that the discrepancy in hydroclimate is associated with changes in the large-scale Rossby-wave pattern and its vertically coupled circulation. The RWS anomalies over South and East Asia further suggest that diabatically forced wave activity contributes to the downstream circulation response. The results therefore indicate that the difference between the two aerosol-response estimates is expressed not only locally through changes in surface temperature and precipitation, but also through changes in the hemispheric upper-level circulation and waveguide.

During 2030–2050 relative to 1965–1985, the upper-tropospheric response is substantially amplified, and the differences between AAER and ALL−xAER become particularly pronounced over the Pacific and, to a lesser extent, the Atlantic–European sector (Fig. 6d–f). In AAER, the zonal-wind response is dominated by broad weakening of the Northern Hemisphere midlatitude jets, particularly along their southern flanks and across the Pacific (Fig. 6d). Weak strengthening along the northern flank and entrance region of the Atlantic jet, together with positive anomalies north of the Pacific jet core, indicates a modest poleward displacement superimposed on the overall jet weakening. The persistence of substantial weakening reflects the continued increase in Asian aerosol forcing, which offsets part of the warming-related strengthening of the midlatitude circulation associated with declining aerosol forcing over Europe and North America.

The ALL−xAER response is stronger and more spatially coherent (Fig. 6e), with extensive weakening along the jet axes and southern flanks and strengthening to the north, particularly over the North Pacific. The difference field therefore highlights

https://doi.org/10.5194/egusphere-2026-5006
Preprint. Discussion started: 31 August 2026

several major changes relative to AAER: weakening of the Asian jet over the continent, a pronounced poleward displacement over the North Pacific, and a contrasting response of the Atlantic jet, which strengthens and shifts poleward over North America but weakens towards Europe (Fig. 6f). These differences reflect the combined influence of the evolving non-aerosol-forced background state and the changing geographical distribution of aerosol forcing, which together modify the meridional temperature gradients that control jet position and strength. The much larger Pacific response compared with the historical transition is consistent with the increasing importance of Asian, rather than predominantly European and North American, aerosol forcing during the future period.

The streamfunction response retains a hemispheric quasi-stationary Rossby-wave structure with zonal wavenumber 4–5 in both experiments, but its amplitude and spatial organisation differ substantially from the historical transition (Fig. 7d–f). The dominant action centres are reorganised, with stronger anomalies over Eurasia, the North Pacific, and North America, while the Atlantic–European sector becomes less dominant. The wave pattern therefore remains hemispheric in scale rather than being confined to the regions of strongest aerosol forcing. Instead, changes in the forcing distribution and background climate state modify the amplitude, phase, and propagation pathways of the large-scale teleconnection.

In AAER, WAF propagation is relatively weak over Europe but becomes more pronounced across northern Eurasia and the Pacific sector. A wave-activity pathway extends from northern Eurasia towards East Asia and Japan before branching into the Pacific, with one branch propagating into the subtropical central Pacific and another extending northeastward across North America and the North Atlantic before weakening over western Europe. Pronounced WAF divergence occurs over northeastern Europe, northern Asia, and northeastern Canada, while equatorward propagation from East Asia into the subtropical Pacific indicates strong interaction between the Asian jet and the tropical circulation. This pathway is consistent with the RWS response, which shows a pronounced positive anomaly over South and East Asia associated with anomalous upper-level divergent outflow accompanying enhanced monsoon convection (Figs. 8d–f and 9d–f). The correspondence between RWS and downstream WAF therefore supports a role for tropical diabatic heating in exciting Rossby-wave activity that subsequently propagates into the extratropics.

The ALL−xAER response retains a broadly similar hemispheric wave-train structure but exhibits stronger and more coherent propagation across northern Europe and Eurasia. WAF propagation from Europe and northern Eurasia extends downstream across the Pacific and North America, while a secondary pathway emerges from central and eastern China, consistent with the corresponding RWS anomaly. The stronger coherence of the wave pattern is consistent with the modified jet structure diagnosed above: the warmer background state produces a different upper-tropospheric waveguide that alters the propagation of Rossby-wave activity. Thus, the difference between ALL−xAER and AAER does not primarily reflect the emergence of an entirely different wave source, but rather a modification of the large-scale circulation response and wave propagation characteristics under a different background climate state.

https://doi.org/10.5194/egusphere-2026-5006
Preprint. Discussion started: 31 August 2026

The upper-tropospheric circulation anomalies again exhibit a coherent three-dimensional structure. In ALL−xAER, strong warming over northern Eurasia is accompanied by an upper-level circulation anomaly and corresponding vertical-motion response that project onto the near-surface pressure and temperature anomalies. Similar vertical consistency is evident over North America, where upper-level circulation anomalies are associated with corresponding surface pressure and temperature responses. Over the Atlantic sector, the upper-level circulation likewise projects onto the surface response, linking changes in the jet structure and wave pattern to the regional SLP, wind, and SST anomalies discussed in the following sections.

Overall, the upper-tropospheric response demonstrates that the divergence between AAER and ALL−xAER is associated with a reorganisation of the hemispheric circulation rather than simply a change in the amplitude of the aerosol response. During the historical transition, the two experiments share a broadly similar Rossby-wave structure, with differences primarily in the strength and position of the jet and waveguide. During the future transition, these differences become substantially larger: changes in the background climate and the geographical distribution of aerosol forcing modify the jet structure, RWS, and downstream propagation of Rossby-wave activity. These changes provide a dynamical pathway linking the different experimental estimates of aerosol forcing to the contrasting regional hydroclimate responses identified above.

3.4 North Atlantic anomalies

The differences between the upper-level circulation responses in ALL−xAER and AAER occur alongside pronounced differences in the North Atlantic climate system. Previous analysis of CESM2 single-forcing experiments has shown that the aerosol response inferred from ALL−xAER is not necessarily dynamically equivalent to the directly simulated aerosol response, with nonlinear coupled interactions involving the North Atlantic and Atlantic Meridional Overturning Circulation (AMOC) contributing to the divergence between the two estimates, particularly during the twenty-first century (Simpson et al., 2023). We therefore examine the corresponding SST and AMOC responses to determine whether the North Atlantic provides an additional coupled component of the circulation differences identified above.

During 2030–2050 relative to 1965–1985, the SST response exhibits pronounced differences between AAER and ALL−xAER over the North Atlantic (Fig. 10). ALL−xAER produces substantial warming over the western and subpolar North Atlantic, with the largest anomalies centred in the subpolar gyre south of Greenland. The nonlinear difference shows a similar spatial structure, indicating that this warming contributes strongly to the divergence between the two aerosol-response estimates. In contrast, AAER produces comparatively weak cooling over much of the subpolar North Atlantic, with its strongest positive anomalies located farther west near northeastern Canada. The stronger warming in ALL−xAER is spatially consistent with a greater oceanic heat transport response and stronger overturning circulation, although the SST and AMOC anomalies do not scale proportionally, indicating that additional air–sea processes contribute to the surface temperature response.

https://doi.org/10.5194/egusphere-2026-5006
Preprint. Discussion started: 31 August 2026

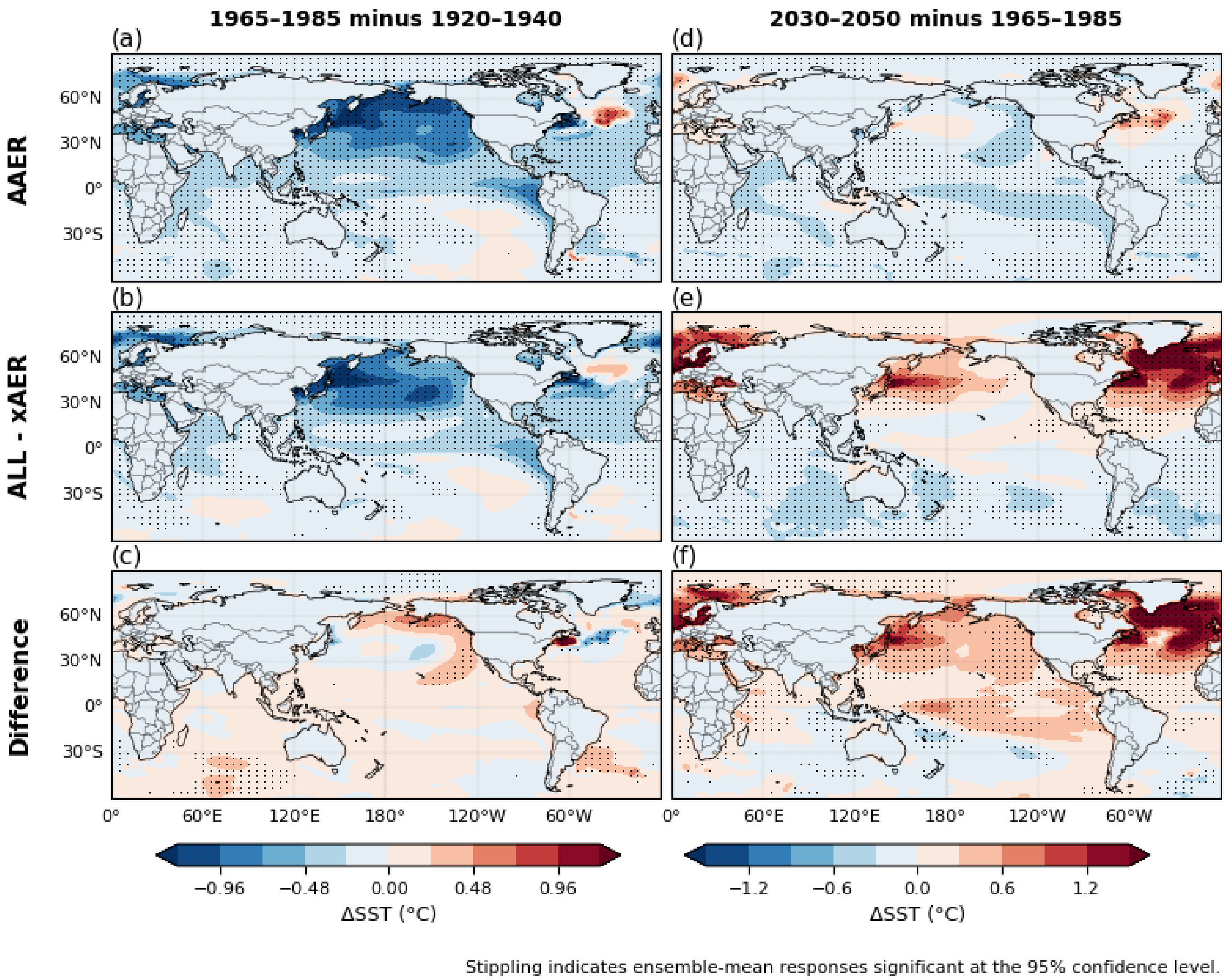

595 **Figure 10. Difference in JJA mean sea surface temperature (ΔSST, °C) between two different periods: 1965–1985 relative to 1920–1940 (left) and 2030–2050 relative to 1965–1985 (right). (a), (d) AAER, (b), (e) ALL-xAER, and (c), (f) the difference between them (ALL-xAER minus AAER). Stippling indicates anomalies that are statistically significant at the 95% confidence level.**

https://doi.org/10.5194/egusphere-2026-5006
Preprint. Discussion started: 31 August 2026

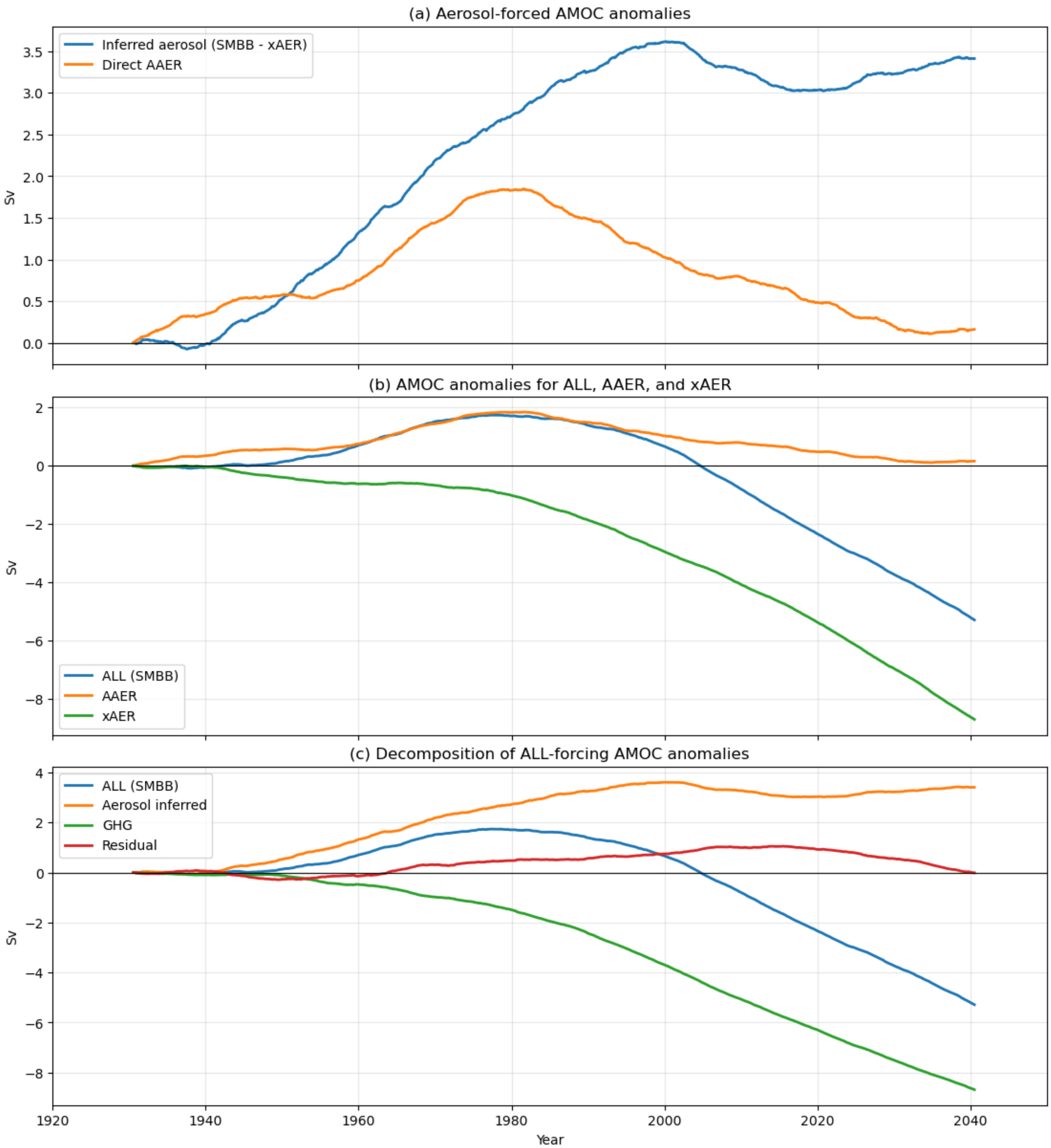

600 **Figure 11. The 21-year running-mean Atlantic Meridional Overturning Circulation (AMOC) anomalies relative to 1920–1940, where the AMOC is defined as the magnitude of the maximum meridional overturning streamfunction below 500 m depth in the North Atlantic at 45°N. (a) Comparison between the aerosol response inferred from ALL−xAER and the directly simulated AAER response. (b) AMOC anomalies in the individual ALL, AAER, and xAER experiments. (c) Decomposition of the ALL-forcing AMOC anomaly into the inferred aerosol contribution (ALL−xAER), the GHG contribution, and a residual term.**

https://doi.org/10.5194/egusphere-2026-5006
Preprint. Discussion started: 31 August 2026

The AMOC evolution provides a complementary perspective on this divergence (Fig. 11). In AAER, the AMOC strengthens by approximately 1.8 Sv around 1980 before declining through the twenty-first century, broadly consistent with the weakening of Northern Hemisphere aerosol forcing after its late-twentieth-century maximum. In contrast, the ALL−xAER response exhibits a substantially larger strengthening, reaching approximately 3.8 Sv in the early 2000s before remaining comparatively stable. Thus, the difference between the two diagnosed aerosol responses continues to increase after the period of maximum aerosol forcing, consistent with the nonlinear coupled behaviour identified by Simpson et al. (2023).

The contrasting AMOC evolution becomes clearer when the individual ALL and xAER experiments are considered separately. Both experiments exhibit an overall weakening of the AMOC during the twenty-first century, consistent with the influence of greenhouse-gas warming and the reduction of Northern Hemisphere aerosol emissions. However, their temporal evolution differs substantially. In ALL, the AMOC continues to strengthen until the early 2000s before weakening, whereas xAER exhibits a more gradual decline over the same period. The difference between these two trajectories therefore produces an ALL−xAER response that continues to increase after the aerosol forcing has reached its late-twentieth-century maximum. By contrast, the direct AAER response begins to weaken after this maximum. The continued evolution of the residual aerosol response therefore reflects not simply the contemporaneous change in aerosol forcing, but also the different evolution of the coupled climate system in ALL and xAER.

The associated atmospheric anomalies provide further evidence that the North Atlantic response is embedded within the broader coupled circulation changes. During 2030–2050, the nonlinear difference is characterised by reduced cloud fraction over the subpolar North Atlantic, primarily due to decreases in low-level clouds. These anomalies coincide spatially with enhanced SST warming and positive shortwave cloud-forcing anomalies (Figs. S8f–S10f), indicating a coherent surface radiative response. The region also exhibits subsidence (and reduced freshwater flux) and anomalous near-surface cyclonic circulation relative to AAER, consistent with the upper-level circulation changes described above. Enhanced near-surface winds may additionally contribute to increased evaporation and surface heat loss (Fig. S11f). Together, these anomalies indicate substantial coupling between the atmospheric circulation, surface radiative balance, and ocean state in the North Atlantic, although the available diagnostics do not establish the direction of causality among these processes.

The comparison of the individual experiments further indicates that the nonlinear difference is substantially influenced by the contrasting evolution of ALL and xAER. Although both experiments exhibit broadly similar large-scale SST and circulation structures, their anomaly centres differ in both location and amplitude. These differences occur alongside changes in the upper-level jet configuration and regional baroclinicity, suggesting that the presence of concurrent greenhouse-gas forcing modifies the background state in which the aerosol forcing operates and thereby alters the coupled North Atlantic response.

https://doi.org/10.5194/egusphere-2026-5006
Preprint. Discussion started: 31 August 2026

The North Atlantic therefore represents an important component of the divergence between the direct and residual-based aerosol responses. During the future transition, ALL−xAER is characterised by stronger subpolar North Atlantic warming and a larger AMOC response than AAER, while the associated changes in cloudiness, surface radiation, circulation, and air–sea exchange are consistent with a coupled ocean–atmosphere adjustment. This North Atlantic response is dynamically connected to the broader hemispheric circulation anomalies identified in Sect.s 3.2 and 3.3 and provides an additional pathway through which the evolving background climate state can influence the diagnosed aerosol response. The interpretation is consistent with Liu et al. (2024), who showed that aerosol-induced upper-level teleconnections can be associated with North Atlantic surface climate and AMOC variability. Importantly, however, the present analysis demonstrates spatial and temporal consistency among these components rather than direct causality. Dedicated sensitivity experiments would be required to isolate the individual causal pathways linking AMOC, SST, atmospheric circulation, and precipitation.

4 Discussion and Conclusions

The comparison between the directly simulated anthropogenic aerosol response (AAER) and the residual response inferred from the difference between all-forcing and fixed-aerosol experiments (ALL−xAER) addresses a fundamental but often implicit assumption in forcing attribution: that these two approaches provide dynamically equivalent estimates of the same aerosol contribution. Our results demonstrate that this equivalence cannot be taken for granted. We examine how differences between direct and residual estimates of the aerosol response depend on the evolving background climate state and how these differences are expressed in regional hydroclimate and atmospheric circulation, building on the earlier finding of Simpson et al. (2023) that the two estimates can differ because of nonlinear coupled interactions. These two experiments expose the climate system to aerosol forcing under fundamentally different background states. In AAER, aerosol emissions evolve while other forcings remain fixed at their initial values, whereas ALL−xAER diagnoses the aerosol contribution within a climate system that simultaneously evolves under greenhouse-gas and other anthropogenic forcings. Consequently, the response to a given aerosol perturbation can depend on the state of the coupled climate system in which that perturbation occurs.

This state dependence is evident in the contrasting behaviour of the two periods considered here. During the historical transition from 1920–1940 to 1965–1985, when Northern Hemisphere aerosol loading increases substantially, AAER and ALL−xAER produce broadly similar large-scale responses, particularly in near-surface temperature. Although regional differences are already apparent in precipitation and circulation, the two approaches nevertheless provide a relatively consistent estimate of the aerosol response. During the future transition, however, their responses diverge substantially. This transition is characterised by declining aerosol emissions over Europe and North America but continued increases over South and East Asia, while greenhouse-gas concentrations and the underlying climate state evolve substantially. The resulting differences are particularly pronounced in precipitation and circulation over the Indo-Pacific, South and East Asia, and the tropical Pacific, but extend to Northern Hemisphere temperature and North Atlantic SST and AMOC responses. Thus, the divergence is not

https://doi.org/10.5194/egusphere-2026-5006
Preprint. Discussion started: 31 August 2026

restricted to hydroclimate or to regions of strong aerosol forcing, but reflects a broader reorganisation of the coupled climate response.

A central implication is that the difference between AAER and ALL−xAER should not be interpreted simply as an additional estimate of aerosol-forcing uncertainty. Rather, it provides a measure of the extent to which the diagnosed aerosol response depends on the experimental framework and background climate state. This distinction is important because residual approaches are widely used to infer forcing contributions when dedicated single-forcing simulations are unavailable. Such residuals are physically meaningful: they represent the difference between two evolving coupled climate states and therefore include the response to aerosol forcing as it operates within the full climate system. However, they do not necessarily represent the same physical perturbation as an aerosol-only experiment conducted against a fixed background state.

The mechanisms underlying this divergence involve both atmospheric dynamics and coupled ocean–atmosphere processes. The low-level circulation analysis shows that differences between AAER and ALL−xAER reorganise moisture transport across the Northern Hemisphere, producing substantially different precipitation responses despite broadly comparable aerosol forcing. These circulation differences extend into the upper troposphere, where both experiments exhibit hemispheric quasi-stationary Rossby wave patterns but differ in their amplitude, phase, jet configuration, and propagation pathways. The associated wave activity flux and Rossby wave source anomalies indicate that changes in tropical diabatic heating and the position of the upper-tropospheric jet modify the pathways through which circulation anomalies are transmitted across the hemisphere. The future residual is therefore not simply a scaled version of the direct aerosol response; rather, the atmospheric response is reorganised dynamically as the background climate state changes.

The North Atlantic provides an additional example of this state dependence. During the future transition, ALL−xAER exhibits substantially stronger subpolar North Atlantic warming and a more persistent AMOC strengthening than AAER. These oceanic differences occur together with changes in cloud cover, surface radiative forcing, sea-level pressure, and near-surface circulation, forming a physically coherent coupled response. The AMOC evolution is particularly informative because the residual response continues to increase after the period of maximum aerosol loading, whereas the direct AAER response weakens. This behaviour demonstrates that the evolution of the residual cannot be understood solely from the contemporaneous aerosol forcing. Instead, it reflects differences in the evolution of the coupled climate system between ALL and xAER, including the different greenhouse-gas-forced background states in which the aerosol contribution is diagnosed. The present analysis does not establish whether the ocean or atmosphere provides the initial perturbation, but it demonstrates that their coupled evolution forms an important component of the divergence between the two attribution approaches.

These findings are related to, but distinct from, the broader literature on nonlinear interactions among climate forcings. Previous studies have demonstrated that the combined response to greenhouse gases and aerosols can depart from the sum of

https://doi.org/10.5194/egusphere-2026-5006
Preprint. Discussion started: 31 August 2026

their separately forced responses through processes involving clouds, surface albedo, atmospheric structure, and ocean circulation (Feichter et al., 2004; Ming and Ramaswamy, 2009; Ming et al., 2011). More recent work has shown that nonlinear residuals can be relatively modest for global-mean quantities while remaining substantial at regional and seasonal scales, particularly for hydroclimate (Deng et al., 2020; Deng, 2025). Our analysis addresses a related but different question. Rather than asking whether the combined response can be reconstructed from the sum of separately forced responses, we ask whether two experimental strategies commonly used to estimate the contribution of an individual forcing produce the same response. The results show that they need not, even when the differences between forcing responses may appear modest at the global scale.

This distinction is particularly relevant for aerosol forcing because its strong spatial heterogeneity makes the response highly dependent on circulation, moisture transport, and regional ocean–atmosphere coupling. Aerosol forcing can also affect remote regions through stationary wave responses and changes in tropical convection and monsoon circulation (Liu et al., 2018; Wilcox et al., 2019; Herbert et al., 2022; Sun et al., 2026). Our results extend this perspective by showing that the diagnosed aerosol signal itself can depend on the experimental framework used to isolate it. Consequently, differences between direct and residual estimates may reflect not only nonlinear interactions among forcings, but also the dependence of the response to a given forcing on the evolving climate state in which it is applied.

The implications are particularly important for regional attribution. Residual estimates such as ALL−xAER remain valuable because they quantify the aerosol contribution within a fully evolving climate system and therefore may be more representative of the perturbation operating in the real world or in a future scenario. Conversely, dedicated aerosol-only experiments provide a cleaner measure of the response to changing aerosol emissions in isolation. The two approaches therefore answer subtly different physical questions. For global-mean quantities, the distinction may be relatively small, but for regional and seasonal climate, especially precipitation and circulation, it can become substantial. Our results further demonstrate that the issue is not restricted to hydroclimate: substantial differences in surface temperature also emerge once the background climate state has evolved sufficiently.

Several limitations should be acknowledged. First, the analysis is based on a single coupled model, CESM2, and therefore demonstrates climate-state dependence within this model rather than providing a multi-model estimate of aerosol nonlinearity. Aerosol–cloud interactions, aerosol forcing strengths, ocean feedbacks, and background climatological states differ substantially across models, so both the magnitude and potentially the sign of the diagnosed nonlinear response may differ in other model frameworks. Establishing the generality of these results will therefore require analogous experiments across a broader model ensemble. Second, although ensemble means are used throughout, regional circulation and precipitation responses may retain contributions from internal variability, particularly where the forced signal is weak. The close consistency between the spatial patterns obtained using the analysis ensemble sizes and those obtained using the larger available ensembles indicates that the main conclusions are not sensitive to ensemble size and that internal variability is sufficiently sampled for the large-scale signals considered here. Nevertheless, regional differences in amplitude and significance remain possible, particularly for the smaller xAER ensemble.

Third, the analysis focuses on JJA and on two selected forcing transitions. The magnitude and structure of the nonlinear response may differ across seasons and across other stages of the historical and future forcing evolution. Additional periods and seasons would therefore be useful for determining how general the identified state dependence is. Fourth, xAER fixes anthropogenic aerosol emissions at 1920 levels rather than at a fully pre-industrial baseline, which may influence the magnitude of the inferred aerosol contribution. Finally, although the diagnostics reveal coherent relationships among North Atlantic SST, AMOC, atmospheric circulation, and precipitation, they remain diagnostic rather than causal. Dedicated sensitivity experiments, including targeted ocean perturbations or SST-restoring experiments, would be required to isolate the direction and strength of the causal pathways linking these components.

Overall, our results demonstrate that the directly simulated aerosol response in AAER and the residual aerosol response inferred from ALL−xAER cannot be assumed to be dynamically equivalent, particularly once the coupled climate system has evolved substantially under greenhouse-gas forcing. In CESM2, the divergence between the two estimates provides a clear indication of climate-state dependence in the aerosol response, expressed through changes in atmospheric circulation, Rossby-wave propagation, moisture transport, and coupled North Atlantic dynamics. The key implication is therefore not that one attribution approach is inherently preferable to the other, but that they quantify aerosol effects under different background conditions and can answer different physical questions. Coordinated large-ensemble single-forcing experiments and targeted regional aerosol perturbation experiments, including LESFMIP and RAMIP (Smith et al., 2022; Wilcox et al., 2023), will be important for establishing whether the state dependence identified here is robust across models, forcing pathways, and regions, and for improving the interpretation of aerosol contributions to regional climate change.

Code and data availability

The analysis scripts used to process the model output, perform the statistical analyses, and produce the figures and diagnostics in this study are available from the corresponding author upon reasonable request. The CESM2 Large Ensemble data used in this study are publicly available through the NSF NCAR Geoscience Data Exchange (GDEX; https://doi.org/10.26024/KGMP-C556). The CESM2 Single-Forcing Large Ensemble data are also publicly available through GDEX (https://doi.org/10.26024/YW4W-1W27). Additional processed data used to produce the figures in this study are available from the corresponding author upon reasonable request.

https://doi.org/10.5194/egusphere-2026-5006
Preprint. Discussion started: 31 August 2026

Author contributions

TZ designed the study, performed the data analysis, produced the figures, and wrote the initial manuscript draft. MAB contributed to the conceptual development of the study, interpretation of the results, and revision of the manuscript.

Competing interests

The authors declare that they have no conflict of interest.

Disclaimer

Publisher's note: Copernicus Publications remains neutral with regard to jurisdictional claims made in the text, published maps, institutional affiliations, or any other geographical representation in this paper. The authors bear the ultimate responsibility for providing appropriate place names. Views expressed in the text are those of the authors and do not necessarily reflect the views of the publisher.

Acknowledgements

The authors acknowledge the Community Earth System Model (CESM) project and the National Science Foundation National Center for Atmospheric Research (NSF NCAR) for producing and making available the CESM2 Large Ensemble and CESM2 Single-Forcing Large Ensemble simulations.

Financial support

We acknowledge support from the UK Natural Environment Research Council (NERC) grant NE/N006038/1.

https://doi.org/10.5194/egusphere-2026-5006
Preprint. Discussion started: 31 August 2026

References

Allen, R. J., Norris, J. R., and Kovilakam, M.: Influence of anthropogenic aerosols and the Pacific Decadal Oscillation on tropical belt width, Nat. Geosci., 7, 270–274, https://doi.org/10.1038/ngeo2091, 2014.

Bellouin, N., Quaas, J., Gryspeerdt, E., Kinne, S., Stier, P., Watson-Parris, D., Boucher, O., Carslaw, K. S., Christensen, M., Daniau, A.-L., Dufresne, J.-L., Feingold, G., Fiedler, S., Forster, P., Gettelman, A., Haywood, J. M., Lohmann, U., Malavelle, F., Mauritsen, T., McCoy, D. T., Myhre, G., Mülmenstädt, J., Neubauer, D., Possner, A., Rugenstein, M., Sato, Y., Schulz, M., Schwartz, S. E., Sourdeval, O., Storelvmo, T., Toll, V., Winker, D., and Stevens, B.: Bounding global aerosol radiative forcing of climate change, Rev. Geophys., 58, e2019RG000660, https://doi.org/10.1029/2019RG000660, 2020.

Bogenschutz, P. A., Gettelman, A., Hannay, C., Larson, V. E., Neale, R. B., Craig, C., and Chen, C.-C.: The path to CAM6: coupled simulations with CAM5.4 and CAM5.5, Geosci. Model Dev., 11, 235–255, https://doi.org/10.5194/gmd-11-235-2018, 2018.

Bollasina, M. A., Ming, Y., and Ramaswamy, V.: Anthropogenic aerosols and the weakening of the South Asian summer monsoon, Science, 334, 502–505, https://doi.org/10.1126/science.1204994, 2011.

Danabasoglu, G., Bates, S. C., Briegleb, B. P., Jayne, S. R., Jochum, M., Large, W. G., Peacock, S., and Yeager, S. G.: The CCSM4 ocean component, J. Climate, 25, 1361–1389, https://doi.org/10.1175/JCLI-D-11-00091.1, 2012.

Danabasoglu, G., Lamarque, J.-F., Bacmeister, J., Bailey, D. A., DuVivier, A. K., Edwards, J., Emmons, L. K., Fasullo, J., Garcia, R., Gettelman, A., Hannay, C., Holland, M. M., Large, W. G., Lauritzen, P. H., Lawrence, D. M., Lenaerts, J. T. M., Lindsay, K., Lipscomb, W. H., Mills, M. J., Neale, R., Oleson, K. W., Otto-Bliesner, B., Phillips, A. S., Sacks, W., Tilmes, S., van Kampenhout, L., Vertenstein, M., Bertini, A., Dennis, J., Deser, C., Fischer, C., Fox-Kemper, B., Kay, J. E., Kinnison, D., Kushner, P. J., Larson, V. E., Long, M. C., Mickelson, S., Moore, J. K., Nienhouse, E., Polvani, L., Rasch, P. J., and Strand, W. G.: The Community Earth System Model Version 2 (CESM2), J. Adv. Model. Earth Syst., 12, e2019MS001916, https://doi.org/10.1029/2019MS001916, 2020.2

Deng, J., Dai, A., and Xu, H.: Nonlinear climate responses to increasing CO2 and anthropogenic aerosols simulated by CESM1, J. Climate, 33, 281–301, https://doi.org/10.1175/JCLI-D-19-0195.1, 2020.

Deng, J.: Nonlinear influence of coexisting CO2 and anthropogenic aerosols on East Asian summer precipitation through a mid-high-latitude pathway, Environ. Res. Lett., 20, 124035, https://doi.org/10.1088/1748-9326/ae20a8, 2025.

DeRepentigny, P., Jahn, A., Holland, M. M., Kay, J. E., Fasullo, J., Lamarque, J.-F., Tilmes, S., Hannay, C., Mills, M. J., Bailey, D. A., and Barrett, A. P.: Enhanced simulated early 21st century Arctic sea ice loss due to CMIP6 biomass burning emissions, Sci. Adv., 8, eabo2405, https://doi.org/10.1126/sciadv.abo2405, 2022.

Dong, B., Wilcox, L. J., Highwood, E. J., and Sutton, R. T.: Impacts of recent decadal changes in Asian aerosols on the East Asian summer monsoon: roles of aerosol–radiation and aerosol–cloud interactions, Clim. Dynam., 53, 3235–3256, https://doi.org/10.1007/s00382-019-04698-0, 2019.

https://doi.org/10.5194/egusphere-2026-5006
Preprint. Discussion started: 31 August 2026

Eyring, V., Bony, S., Meehl, G. A., Senior, C. A., Stevens, B., Stouffer, R. J., and Taylor, K. E.: Overview of the Coupled Model Intercomparison Project Phase 6 (CMIP6) experimental design and organization, Geosci. Model Dev., 9, 1937–1958, https://doi.org/10.5194/gmd-9-1937-2016, 2016.

Fasullo, J. T., Lamarque, J.-F., Hannay, C., Rosenbloom, N., Tilmes, S., DeRepentigny, P., Jahn, A., and Deser, C.: Spurious late historical-era warming in CESM2 driven by prescribed biomass burning emissions, Geophys. Res. Lett., 49, e2021GL097420, https://doi.org/10.1029/2021GL097420, 2022.

Feichter, J., Roeckner, E., Lohmann, U., and Liepert, B.: Nonlinear aspects of the climate response to greenhouse gas and aerosol forcing, J. Climate, 17, 2384–2398, https://doi.org/10.1175/1520-0442(2004)017<2384:NAOTCR>2.0.CO;2, 2004.

Gettelman, A. and Morrison, H.: Advanced two-moment bulk microphysics for global models. Part I: Off-line tests and comparison with other schemes, J. Climate, 28, 1268–1287, https://doi.org/10.1175/JCLI-D-14-00102.1, 2015.

Gillett, N. P., Shiogama, H., Funke, B., Hegerl, G., Knutti, R., Matthes, K., Santer, B. D., Stone, D., and Tebaldi, C.: The Detection and Attribution Model Intercomparison Project (DAMIP v1.0) contribution to CMIP6, Geosci. Model Dev., 9, 3685–3697, https://doi.org/10.5194/gmd-9-3685-2016, 2016.

Gillett, N. P., Wehner, M. F., Tett, S. F. B., and Weaver, A. J.: Testing the linearity of the response to combined greenhouse gas and sulfate aerosol forcing, Geophys. Res. Lett., 31, L14201, https://doi.org/10.1029/2004GL020111, 2004.

Grise, K. M. and Polvani, L. M.: The response of midlatitude jets to increased CO2: distinguishing the roles of sea surface temperature and direct radiative forcing, Geophys. Res. Lett., 41, 6863–6871, https://doi.org/10.1002/2014GL061638, 2014.

Guo, L., Highwood, E. J., Shaffrey, L. C., and Turner, A. G.: The effect of regional changes in anthropogenic aerosols on rainfall of the East Asian Summer Monsoon, Atmos. Chem. Phys., 13, 1521–1534, https://doi.org/10.5194/acp-13-1521-2013, 2013.

Herbert, R., Wilcox, L. J., Joshi, M., Highwood, E., and Frame, D.: Nonlinear response of Asian summer monsoon precipitation to emission reductions in South and East Asia, Environ. Res. Lett., 17, 014005, https://doi.org/10.1088/1748-9326/ac3b19, 2022.

Hoesly, R. M., Smith, S. J., Feng, L., Klimont, Z., Janssens-Maenhout, G., Pitkanen, T., Seibert, J. J., Vu, L., Andres, R. J., Bolt, R. M., Bond, T. C., Dawidowski, L., Kholod, N., Kurokawa, J.-I., Li, M., Liu, L., Lu, Z., Moura, M. C. P., O'Rourke, P. R., and Zhang, Q.: Historical (1750–2014) anthropogenic emissions of reactive gases and aerosols from the Community Emissions Data System (CEDS), Geosci. Model Dev., 11, 369–408, https://doi.org/10.5194/gmd-11-369-2018, 2018.

Hunke, E. C., Lipscomb, W. H., Turner, A. K., Jeffery, N., and Elliott, S.: CICE: The Los Alamos Sea Ice Model Documentation and Software User's Manual, Version 5.1, Los Alamos National Laboratory, Los Alamos, NM, USA, LA-CC-06-012, 2015.

Hwang, Y.-T., Frierson, D. M. W., and Kang, S. M.: Anthropogenic sulfate aerosol and the southward shift of tropical precipitation in the late 20th century, Geophys. Res. Lett., 40, 2845–2850, https://doi.org/10.1002/grl.50502, 2013.

https://doi.org/10.5194/egusphere-2026-5006
Preprint. Discussion started: 31 August 2026

IPCC: Climate Change 2021: The Physical Science Basis, Contribution of Working Group I to the Sixth Assessment Report of the Intergovernmental Panel on Climate Change, edited by: Masson-Delmotte, V., Zhai, P., Pirani, A., Connors, S. L., Péan, C., Berger, S., Caud, N., Chen, Y., Goldfarb, L., Gomis, M. I., Huang, M., Leitzell, K., Lonnoy, E., Matthews, J. B. R., Maycock, T. K., Waterfield, T., Yelekçi, O., Yu, R., and Zhou, B., Cambridge University Press, Cambridge, UK and New York, NY, USA, 2391 pp., https://doi.org/10.1017/9781009157896, 2021.

Jones, G. S., Stott, P. A., and Mitchell, J. F. B.: Uncertainties in the attribution of greenhouse gas warming and implications for climate prediction, J. Geophys. Res.-Atmos., 121, 6969–6992, https://doi.org/10.1002/2015JD024337, 2016.

Lau, W. K.-M. and Kim, K.-M.: Competing influences of greenhouse warming and aerosols on Asian summer monsoon circulation and rainfall, Asia-Pac. J. Atmos. Sci., 53, 181–194, https://doi.org/10.1007/s13143-017-0033-4, 2017.

Lawrence, D. M., Fisher, R. A., Koven, C. D., Oleson, K. W., Swenson, S. C., Bonan, G., Collier, N., Ghimire, B., van Kampenhout, L., Kennedy, D., Kluzek, E., Lawrence, P. J., Li, F., Li, H., Lombardozzi, D., Riley, W. J., Sacks, W. J., Shi, M., Vertenstein, M., Wieder, W. R., Xu, C., Ali, A. A., Badger, A. M., Bisht, G., van den Broeke, M., Brunke, M. A., Burns, S. P., Buzan, J., Clark, M., Craig, A., Dahlin, K., Drewniak, B., Fisher, J. B., Flanner, M., Fox, A. M., Gentine, P., Hoffman, F., Keppel-Aleks, G., Knox, R., Kumar, S., Lenaerts, J., Leung, L. R., Lipscomb, W. H., Lu, Y., Pandey, A., Pelletier, J. D., Perket, J., Randerson, J. T., Ricciuto, D. M., Sanderson, B. M., Slater, A., Subin, Z. M., Tang, J., Thomas, R. Q., Val Martin, M., and Zeng, X.: The Community Land Model Version 5: Description of new features, benchmarking, and impact of forcing uncertainty, J. Adv. Model. Earth Syst., 11, 4245–4287, https://doi.org/10.1029/2018MS001583, 2019.

Li, Z., Lau, W. K., Ramanathan, V., Wu, G., Ding, Y., Manoj, M. G., Liu, J., Qian, Y., Li, J., Zhou, T., Fan, J., Rosenfeld, D., Ming, Y., Wang, Y., Huang, J., Wang, B., Xu, X., Lee, S., Cribb, M., Zhang, F., Yang, X., Zhao, C., Takemura, T., Wang, K., Xia, X., Yin, Y., Zhang, H., Guo, J., Zhai, P. M., Sugimoto, N., Babu, S. S., and Brasseur, G. P.: Aerosol and monsoon climate interactions over Asia, Rev. Geophys., 54, 866–929, https://doi.org/10.1002/2015RG000500, 2016.

Liu, L., Shawki, D., Voulgarakis, A., Kasoar, M., Samset, B. H., Myhre, G., Forster, P. M., Hodnebrog, Ø., Sillmann, J., Aalbergsjø, S. G., Boucher, O., Faluvegi, G., Iversen, T., Kirkevåg, A., Lamarque, J.-F., Olivié, D., Richardson, T., Shindell, D., and Takemura, T.: A PDRMIP multimodel study on the impacts of regional aerosol forcings on global and regional precipitation, J. Climate, 31, 4429–4447, https://doi.org/10.1175/JCLI-D-17-0439.1, 2018.

Liu, X., Ma, P.-L., Wang, H., Tilmes, S., Singh, B., Easter, R. C., Ghan, S. J., and Rasch, P. J.: Description and evaluation of a new four-mode version of the Modal Aerosol Module (MAM4) within version 5.3 of the Community Atmosphere Model, Geosci. Model Dev., 9, 505–522, https://doi.org/10.5194/gmd-9-505-2016, 2016.

Liu, Z., Bollasina, M. A., and Wilcox, L. J.: Impact of Asian aerosols on the summer monsoon strongly modulated by regional precipitation biases, Atmos. Chem. Phys., 24, 7227–7252, https://doi.org/10.5194/acp-24-7227-2024, 2024.

Lund, M. T., Myhre, G., and Samset, B. H.: Anthropogenic aerosol forcing under the Shared Socioeconomic Pathways, Atmos. Chem. Phys., 19, 13827–13839, https://doi.org/10.5194/acp-19-13827-2019, 2019.

Meinshausen, M., Nicholls, Z. R. J., Lewis, J., Gidden, M. J., Vogel, E., Freund, M., Beyerle, U., Gessner, C., Nauels, A., Bauer, N., Canadell, J. G., Daniel, J. S., John, A., Krummel, P. B., Luderer, G., Meinshausen, N., Montzka, S. A., Rayner, P.

J., Reimann, S., Smith, S. J., van den Berg, M., Velders, G. J. M., Vollmer, M. K., and Wang, R. H. J.: The shared socio-economic pathway (SSP) greenhouse gas concentrations and their extensions to 2500, Geosci. Model Dev., 13, 3571–3605, https://doi.org/10.5194/gmd-13-3571-2020, 2020.

Meinshausen, M., Vogel, E., Nauels, A., Lorbacher, K., Meinshausen, N., Etheridge, D. M., Fraser, P. J., Montzka, S. A., Rayner, P. J., Trudinger, C. M., Krummel, P. B., Beyerle, U., Canadell, J. G., Daniel, J. S., Enting, I. G., Law, R. M., Lunder, C. R., O'Doherty, S., Prinn, R. G., Reimann, S., Rubino, M., Velders, G. J. M., Vollmer, M. K., Wang, R. H. J., and Weiss, R.: Historical greenhouse gas concentrations for climate modelling (CMIP6), Geosci. Model Dev., 10, 2057–2116, https://doi.org/10.5194/gmd-10-2057-2017, 2017.

Ming, Y. and Ramaswamy, V.: Nonlinear climate and hydrological responses to aerosol effects, J. Climate, 22, 1329–1339, https://doi.org/10.1175/2008JCLI2362.1, 2009.

Ming, Y., Ramaswamy, V., and Chen, G.: A model investigation of aerosol-induced changes in boreal winter extratropical circulation, J. Climate, 24, 6077–6091, https://doi.org/10.1175/2011JCLI4111.1, 2011.

Mitchell, J. F. B., Johns, T. C., Gregory, J. M., and Tett, S. F. B.: Climate response to increasing levels of greenhouse gases and sulphate aerosols, Nature, 376, 501–504, https://doi.org/10.1038/376501a0, 1995.

Needham, M. R. and Randall, D. A.: Anomalous northward energy transport due to anthropogenic aerosols during the twentieth century, J. Climate, 36, 6713–6728, https://doi.org/10.1175/JCLI-D-22-0798.1, 2023.

Needham, M. R., Cox, T., and Randall, D. A.: Aerosol-induced changes in atmospheric and oceanic heat transports in the CESM2 Large Ensemble, J. Climate, 37, 6395–6412, https://doi.org/10.1175/JCLI-D-23-0455.1, 2024.

Persad, G. G. and Caldeira, K.: Divergent global-scale temperature effects from identical aerosols emitted in different regions, Nat. Commun., 9, 3289, https://doi.org/10.1038/s41467-018-05838-6, 2018.

Recchia, L. G. and Lucarini, V.: Modelling the effect of aerosol and greenhouse gas forcing on the South and East Asian monsoons with an intermediate-complexity climate model, Earth Syst. Dynam., 14, 697–722, https://doi.org/10.5194/esd-14-697-2023, 2023.

Rodgers, K. B., Lee, S.-S., Rosenbloom, N., Timmermann, A., Danabasoglu, G., Deser, C., Edwards, J., Kim, J.-E., Simpson, I. R., Stein, K., Stuecker, M. F., Yamaguchi, R., Bódai, T., Chung, E.-S., Huang, L., Kim, W. M., Lamarque, J.-F., Lombardozzi, D. L., Wieder, W. R., and Yeager, S. G.: Ubiquity of human-induced changes in climate variability, Earth Syst. Dynam., 12, 1393–1411, https://doi.org/10.5194/esd-12-1393-2021, 2021.

Samset, B. H., Sand, M., Smith, C. J., Bauer, S. E., Forster, P. M., Fuglestvedt, J. S., Osprey, S., and Schleussner, C.-F.: Climate impacts from a removal of anthropogenic aerosol emissions, Geophys. Res. Lett., 45, 1020–1029, https://doi.org/10.1002/2017GL076079, 2018.

Shawki, D., Voulgarakis, A., Chakraborty, A., Kasoar, M., and Srinivasan, J.: The South Asian monsoon response to remote aerosols: global and regional mechanisms, J. Geophys. Res.-Atmos., 123, 11585–11601, https://doi.org/10.1029/2018JD028623, 2018.

https://doi.org/10.5194/egusphere-2026-5006
Preprint. Discussion started: 31 August 2026

Shindell, D. T., Voulgarakis, A., Faluvegi, G., and Milly, G.: Precipitation response to regional radiative forcing, Atmos. Chem. Phys., 12, 6969–6982, https://doi.org/10.5194/acp-12-6969-2012, 2012.

Simpson, I. R., Rosenbloom, N., Danabasoglu, G., Deser, C., Yeager, S. G., McCluskey, C. S., Yamaguchi, R., Lamarque, J.-F., Tilmes, S., Mills, M. J., and Rodgers, K. B.: The CESM2 Single-Forcing Large Ensemble and comparison to CESM1: implications for experimental design, J. Climate, 36, 5687–5711, https://doi.org/10.1175/JCLI-D-22-0666.1, 2023.

Smith, D. M., Gillett, N. P., Simpson, I. R., Athanasiadis, P. J., Baehr, J., Bethke, I., Bilge, T. A., Bonnet, R., Boucher, O., Findell, K. L., Gastineau, G., Gualdi, S., Hermanson, L., Leung, L. R., Mignot, J., Müller, W. A., Osprey, S., Otterå, O. H., Persad, G. G., Scaife, A. A., Schmidt, G. A., Shiogama, H., Sutton, R. T., Swingedouw, D., Yang, S., Zhou, T., and Ziehn, T.: Attribution of multi-annual to decadal changes in the climate system: The Large Ensemble Single Forcing Model Intercomparison Project (LESFMIP), Front. Clim., 4, 955414, https://doi.org/10.3389/fclim.2022.955414, 2022.

Smith, R., Jones, P., Briegleb, B., Bryan, F., Danabasoglu, G., Dennis, J., Dukowicz, J., Eden, C., Fox-Kemper, B., Gent, P., Hecht, M., Jayne, S., Jochum, M., Large, W., Lindsay, K., Maltrud, M., Norton, N., Peacock, S., Vertenstein, M., and Yeager, S.: The Parallel Ocean Program (POP) reference manual: Ocean component of the Community Climate System Model (CCSM) and Community Earth System Model (CESM), Los Alamos National Laboratory Tech. Rep. LAUR-10-01853, Los Alamos, NM, USA, 141 pp., 2010.

Sun, W., Bollasina, M. A., Colfescu, I., Wu, G., and Liu, Y.: European sulphate aerosols were a key driver of the early twentieth-century intensification of the Asian summer monsoon, Atmos. Chem. Phys., 26, 2027–2039, https://doi.org/10.5194/acp-26-2027-2026, 2026.

Szopa, S., Naik, V., Adhikary, B., Artaxo, P., Berntsen, T., Collins, W., Fuzzi, S., Gallardo, L., Kiendler-Scharr, A., Klimont, Z., Liao, H., Unger, N., and Zanis, P.: Short-Lived Climate Forcers, in: Climate Change 2021: The Physical Science Basis, Contribution of Working Group I to the Sixth Assessment Report of the Intergovernmental Panel on Climate Change, Cambridge University Press, Cambridge, UK and New York, NY, USA, 817–922, https://doi.org/10.1017/9781009157896.008, 2021.

Takaya, K. and Nakamura, H.: A formulation of a phase-independent wave-activity flux for stationary and migratory quasigeostrophic eddies on a zonally varying basic flow, J. Atmos. Sci., 58, 608–627, https://doi.org/10.1175/1520-0469(2001)058<0608:AFOAPI>2.0.CO;2, 2001.

Turnock, S. T., Allen, R. J., Andrews, M., Bauer, S. E., Deushi, M., Emmons, L., Good, P., Horowitz, L., John, J. G., Michou, M., Nabat, P., Naik, V., Neubauer, D., O'Connor, F. M., Olivié, D., Oshima, N., Schulz, M., Sellar, A., Shim, S., Takemura, T., Tilmes, S., Tsigaridis, K., Wu, T., and Zhang, J.: Historical and future changes in air pollutants from CMIP6 models, Atmos. Chem. Phys., 20, 14547–14579, https://doi.org/10.5194/acp-20-14547-2020, 2020.

Undorf, S., Polson, D., Bollasina, M. A., Ming, Y., Schurer, A., and Hegerl, G. C.: Detectable impact of local and remote anthropogenic aerosols on the 20th century changes of West African and South Asian monsoon precipitation, J. Geophys. Res.-Atmos., 123, 4871–4889, https://doi.org/10.1029/2017JD027711, 2018.

https://doi.org/10.5194/egusphere-2026-5006
Preprint. Discussion started: 31 August 2026

van Marle, M. J. E., Kloster, S., Magi, B. I., Marlon, J. R., Daniau, A.-L., Field, R. D., Arneth, A., Forrest, M., Hantson, S., Kehrwald, N. M., Knorr, W., Lasslop, G., Li, F., Mangeon, S., Yue, C., Kaiser, J. W., and van der Werf, G. R.: Historic global biomass burning emissions for CMIP6 (BB4CMIP) based on merging satellite observations with proxies and fire models (1750–2015), Geosci. Model Dev., 10, 3329–3357, https://doi.org/10.5194/gmd-10-3329-2017, 2017.

Wilcox, L. J., Allen, R. J., Samset, B. H., Bollasina, M. A., Griffiths, P. T., Keeble, J., Lund, M. T., Makkonen, R., Merikanto, J., O'Donnell, D., Paynter, D. J., Persad, G. G., Rumbold, S. T., Takemura, T., Tsigaridis, K., Undorf, S., and Westervelt, D. M.: The Regional Aerosol Model Intercomparison Project (RAMIP), Geosci. Model Dev., 16, 4451–4479, https://doi.org/10.5194/gmd-16-4451-2023, 2023.

Wilcox, L. J., Dunstone, N., Lewinschal, A., Bollasina, M., Ekman, A. M. L., and Highwood, E. J.: Mechanisms for a remote response to Asian anthropogenic aerosol in boreal winter, Atmos. Chem. Phys., 19, 9081–9095, https://doi.org/10.5194/acp-19-9081-2019, 2019.